AFRL-AFOSR-UK-TR-2015-0043

Development of a ground test concept based on multi-rotors for in-flight RVD experimentation

ELISA CAPELLO
GIORGIO GUGLIERI

POLITECNICO DI TORINO
Dipartimento di Ingegneria Meccanica ed Aerospaziale (DIMEAS)
Corso Duca degli Abruzzi 24
Torino, 10129 ITALY

EOARD Grant #FA2386-14-1-5007

Report Date: August 2015

Final Report from 30 September 2014 to 31 August 2015

Air Force Research Laboratory
Air Force Office of Scientific Research
European Office of Aerospace Research and Development
Unit 4515, APO AE 09421-4515

REPORT DOCUMENTATION PAGE

Form Approved OMB No. 0704-0188

1. REPORT DATE *(DD-MM-YYYY)*	2. REPORT TYPE	3. DATES COVERED *(From – To)*
22 August 2015	Final Report	30 September 2014 – 31 August 2015

4. TITLE AND SUBTITLE

Development of a ground test concept based on multi-rotors for in-flight RVD experimentation

5a. CONTRACT NUMBER

5b. GRANT NUMBER

FA2386-14-1-5007

5c. PROGRAM ELEMENT NUMBER

61102F

6. AUTHOR(S)

ELISA CAPELLO
GIORGIO GUGLIERI

5d. PROJECT NUMBER

5d. TASK NUMBER

5e. WORK UNIT NUMBER

7. PERFORMING ORGANIZATION NAME(S) AND ADDRESS(ES)
POLITECNICO DI TORINO
Dipartimento di Ingegneria Meccanica ed Aerospaziale (DIMEAS)
Corso Duca degli Abruzzi 24
Torino, 10129 ITALY

8. PERFORMING ORGANIZATION REPORT NUMBER

N/A

9. SPONSORING/MONITORING AGENCY NAME(S) AND ADDRESS(ES)

EOARD
Unit 4515
APO AE 09421-4515

10. SPONSOR/MONITOR'S ACRONYM(S)

AFRL/AFOSR/IOE (EOARD)

11. SPONSOR/MONITOR'S REPORT NUMBER(S)

AFRL-AFOSR-UK-TR-2015-0043

12. DISTRIBUTION/AVAILABILITY STATEMENT

Distribution A: Approved for public release; distribution is unlimited.

13. SUPPLEMENTARY NOTES

14. ABSTRACT

The objective of this research is a feasibility study of an L1-based GNC for rendez-vous and docking maneuvers of two systems, including theoretical background and a comprehensive analysis of simulation results.The performance of the proposed GNC design will be evaluated in a simulation environment reproducing the dynamics of a multi-rotor micro-aerial vehicle. The nonlinear and linear models of an hexarotor Unmanned Aerial Vehicle (UAV) are identified using a VICON system. Some simulations are performed to validate the implementation of the nonlinear model in the Matlab-Simulink environment. Two controllers have been implemented: (i) a classical linear quadratic regulator (LQR) and (ii) an L1 adaptive controller. Both controller performance are validated by simulations. Different cases are analyzed, including simulations of experimental flights. The L1 adaptive controller is validated not only for the linear model but also for the nonlinear model and for "realistic" cases in which a time dealy and an actuator model are included. Both controllers guarantee good performance. A retuning of the L1 controller is not required even in presence of time delay and for the nonlinear model.

15. SUBJECT TERMS

EOARD, multirotor UAVs, identification, simulation methods, experimental results, rendez-vous and docking

16. SECURITY CLASSIFICATION OF:			17. LIMITATION OF ABSTRACT	18, NUMBER OF PAGES	19a. NAME OF RESPONSIBLE PERSON
a. REPORT	b. ABSTRACT	c. THIS PAGE			Kent Miller
UNCLAS	UNCLAS	UNCLAS	SAR	42	19b. TELEPHONE NUMBER *(Include area code)* +44 (0)1895 616816

Technical Report
"Development of a ground test concept based on multi-rotors for in-flight RVD experimentation"
DEMO Project - EOARD Grant FA2386-14-1-5007
Period of performance: January-July 2015

Investigator: Prof. Giorgio Guglieri
Co-Investigator: Dr. Elisa Capello

Politecnico di Torino, Dipartimento di Ingegneria Meccanica ed Aerospaziale (DIMEAS), Corso Duca degli Abruzzi 24, 10129 Torino, Italy; e-mail:(giorgio.guglieri, elisa.capello)@polito.it.

Abstract: The objective of this research (EOARD Grant $14-5007$) is a feasibility study of an $\mathcal{L}_1$-based GNC for rendez-vous and docking maneuvers of two systems, including theoretical background and a comprehensive analysis of simulation results. The performance of the proposed GNC design will be evaluated in a simulation environment reproducing the dynamics of a multi-rotor micro-aerial vehicle. The nonlinear and linear models of an hexarotor Unmanned Aerial Vehicle (UAV) are identified using a VICON system. Some simulations are performed to validate the implementation of the nonlinear model in the Matlab-Simulink environment. Two controllers have been implemented: (i) a classical linear quadratic regulator (LQR) and (ii) an $\mathcal{L}_1$ adaptive controller. Both controller performance are validated by simulations. Different cases are analyzed, including simulations of experimental flights. The $\mathcal{L}_1$ adaptive controller is validated not only for the linear model but also for the nonlinear model and for "realistic" cases in which a time dealy and an actuator model are included. Both controllers guarantee good performance. A retuning of the $\mathcal{L}_1$ controller is not required even in presence of time delay and for the nonlinear model.

Keywords: multirotor UAVs, identification, simulation methods, experimental results, rendez-vous and docking

---

Contents

1. INTRODUCTION

The rendez-vous and docking (RVD) maneuver is a key operational technology that is required for many missions, and it consists of a series of orbital maneuvers and controlled trajectories, where an active spacecraft (Chaser) tries to capture a passive Target vehicle or to reach and remove large space debris object. Usually, the goal of the RVD mission is that a Chaser vehicle has to safely and efficiently approach the Target vehicle (that is in a fixed position) to within a few centimeters (surface-to-surface) and remain stationary there until the hold mechanism captures and docks the target vehicle.

Traditionally, rendez-vous and proximity maneuvers have been performed using open loop maneuver planning techniques and ad hoc error corrections. Various constraints arises in these maneuvers including constraints on thrust magnitude, on platform positioning within Line-of-Sight cone while approaching the docking system on a target platform and on approach velocity to match the velocity of the docking port. As pointed out in [31, 25] one reason for considering adaptive methods in these practical applications is to compensate for large variations in plant parameter values. For this reason, in this research an $\mathcal{L}_1$ adaptive controller is proposed, that is robust even when parameters have a high rate of variation [5]. First, this controller ensures uniform transient tracking for both the system inputs and outputs. Second, the adaptation sampling time associated with the sampling rate of the autonomous system [7, 8]. The robustness of this controller is compared with a classical robust control.

The purpose of this research activity is an exploratory study that may provide evidence of the feasibility of the $\mathcal{L}_1$ adaptive controller for docking maneuvers. One problem for the implementation of this algorithm on a mockup or on a real spacecraft is the cost of the platform and of the spacecraft systems. The idea of this model-based research is to reduce development time and cost by eliminating the need for early product prototypes and by narrowing down possible design alternatives early in the process [33, 16]. In a competitive market, actors in technology and engineering industries seek to reduce cost and time consumption for their development processes. For this reason, we propose to implement and validate the adaptive controller on a multi-rotor Unmanned Aerial Vehicle (UAV) that has to dock on a fixed target.

In recent years, researchers have begun to integrate adaptation in the control designs of multirotor UAVs in order to achieve a higher accuracy and robustness in presence of model uncertainties and external disturbances. In [35] a review of several algorithms have been analyzed including their advantages and disadvantages, considering multi-rotor nonlinear nature and under-actuated configuration. Roberts et.al. [28] proposed an adaptive controller for the position tracking of a vertical take-off and landing UAV. The validation of the controller is limited to bounded inputs and outputs, and it is not applied to a nonlinear model.

Our research proposes a model-based design of a multi-rotor UAV, starting from the identification of the model parameters and to use the UAV prototype for technology demonstration. The purpose of this research also includes exploration of position estimation techniques using a VICON system.

Model-based control systems design is a concept where mathematical process models are used to simulate and verify system performance before building physical prototypes. Model-based software design simplifies conventional development using an intuitive block diagram environment and automatic code generation. Model-based development with code generation is claimed to be a promising approach when developing image analysis algorithms towards embedded platforms [10]. MathWorks recently added native support for code generation in Simulink for small singleboard computers powerful enough to perform advanced image analysis algorithms. These platforms are available at consumer price levels and no extra code generating Matlab toolboxes are required.

The model-based design approach using a plant model, achieved through physical modeling and system identification, enabled early verification and validation of control and image analysis algorithms. Identification of different parameters is a time consuming and in many cases expensive processes. Works of [13] show that even though it is possible, it demands a lot of equipment and multiple experiments. The parameters are validated only for hovering, since recreating the condition during forward flight is very difficult. One approach that could prove useful is the one used in [1, 2]. The authors try to identify linear decoupled models with data collected from flight experiments. The problem of this kind of identification is that to perform flight experiments a working feedback controller is needed on-board.

Our idea is to select an open loop identification method of the multi-rotor physical parameters. The novelty of the proposed approach id that a VICON system is considered for identify the system and for the evaluation of the thrust and torque. This approach is chosen to reduce the time of collecting data and to avoid risk of accidents during flight tests considering that a controller is not yet implemented on-board. The nonlinear model, implemented in Matlab-Simulink, is validated with experimental flights of an hexacopter UAV. A linear quadratic regulator and an $\mathcal{L}_1$ adaptive controllers are also implemented considering the identified physical parameters. The performance of both controllers are evaluated by a comprehensive analysis of simulation results. Different cases are analyzed. The robustness of the $\mathcal{L}_1$ adaptive controller is validated with the application to a nonlinear model that includes a time delay on the control channel and an actuator model.

2. MODEL DESCRIPTION

The problem of identification proposed in this paper is applied to a multi rotor UAV with six engines using a VICON system for the measurement of inertia and thrust/torque gains.

2.1 Hexacopter model

We assume that the hexacopter structure is rigid and that the center of mass (CoM) is coincident with the geometrical center (GC). The hexacopter consists of six arms all connected symmetrically to the central hub to simplify the balance of the separate thrusters. Kevlar bars are considered for the structure construction. At the end of each arm a propeller driven by an electric motor is attached. See Figure 1 for the hexarotor system. The hub has to be designed to ensure the correct location and orientation of the struts on assembly and could be a simple under-over clamping system to provide a rugged demountable part. All the propellers have fixed pitch blades, thus the propellers can not be tilted. As indicated in Fig. 2, three propellers rotate anticlockwise and three clockwise.

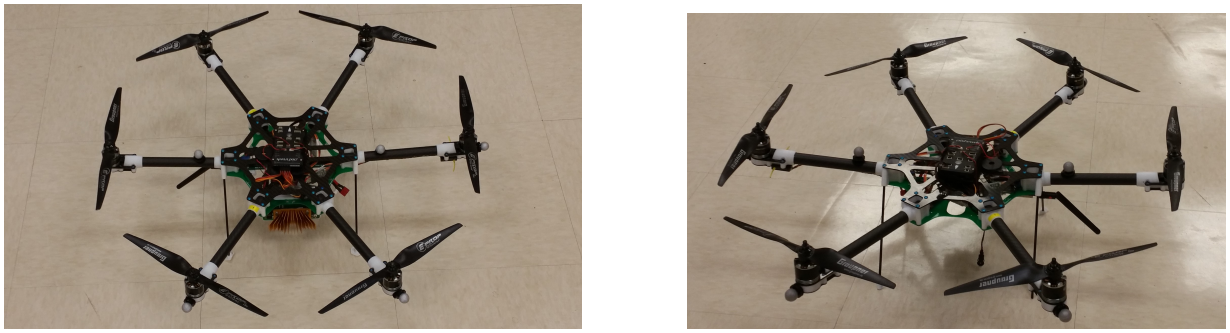

Fig. 1. Hexacopter platform

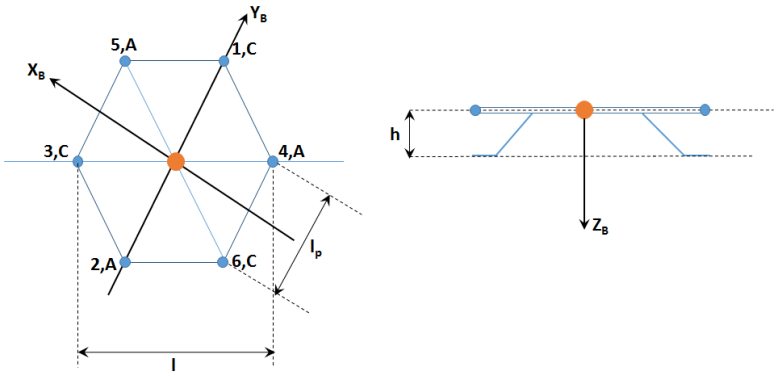

Fig. 2. Hexacopter rotations and body reference frame. A = Anticlockwise, C = Clockwise. (X_B, Y_B, Z_B) is the body reference frame.

Four basic movements are considered varying the thrust produced by each propellers. The rotation of the rotors produce also a reaction torque, opposite of the rotation direction. Since half of the propellers are spinning in one direction, the net torque when all rotors have equal speed is zero.

The main control of the hexacopter is the throttle and it is used for the movements in the body vertical direction. Since the propellers are fixed pitched, the direction of the throttle is fixed and it is used to counter act the gravity. When increasing (decreasing) the throttle, the hexarotor will travel upwards (downwards). Throttle is produced by increasing (decreasing) the speed of all rotors of the same entity.

The second basic movement is related to the roll variation, that is produced by increasing (decreasing) the speed of rotors on right side while decreasing (increasing) the left side rotor speed of the same amount.

The third movement is the pitch variation, that is produced by increasing (decreasing) the rear rotor speed while decreasing (increasing) the front rotor speed.

The yaw movement (fourth basic movement) is produced by increasing (decreasing) the speed of the rotors rotating clockwise while decreasing (increasing) the rotors rotating anticlockwise.

The electric engines are the T-Motor KV 750 (MT2212) with E-prop ultra-light carbon propellers. A radio controller is used to control the hexarotor by sending reference values for controls.

The hexacopter is able to perform autonomous flight thanks to the on board installation of an autopilot, that is the PixHawk, that is a high-performance autopilot-on-module. Its main characteristics comprehend an open architecture, the possibility to be reprogrammed in flight and real time telemetry. The CPU is the 32bit STM32F427 Cortex M4 core with FPU and 2Mb flash memory and 256 kb of RAM with a CPU clock of 168 MHz. The autopilot is placed on the central hub together with the Lithium Polymer (LiPo) battery and the receiver connected to the ground control station.

The characteristics of the hexacopter are in Table 1. The approximate total weight of the multi rotor is 930 gr.

Table 1. Hexacopter Characteristics

Electric motor	T-Motor KV 750 (MT2212)	$m_e = 55$ g
Propeller E-Prop	254 mm x 120 mm	$m_p = 12$ g
LiPo Battery	Thunder Power 1800mAh	$m_b = 155$ g
Structure weight		$m_s = 350$ g
Total weight		$m = 930$ g

2.2 VICON system

For the identification of the inertial and propulsion characteristics, a VICON system is used. The VICON motion capture system is a state-of-the-art infrared marker-tracking system that offers millimeter resolution of 3D spatial displacements. Ten VICON cameras (see Fig. 3) are installed along the walls of the laboratory to collect and stream high quality 3D position and attitude information. The VICON server is able to provide the position and the attitude of a rigid body with a resolution between 0.001 and 0.01 millimeters. The refresh rate is limited only by the streaming rate of the TCP/IP network, while the resolution depends on the distance and number of passive markers on the tracked body.

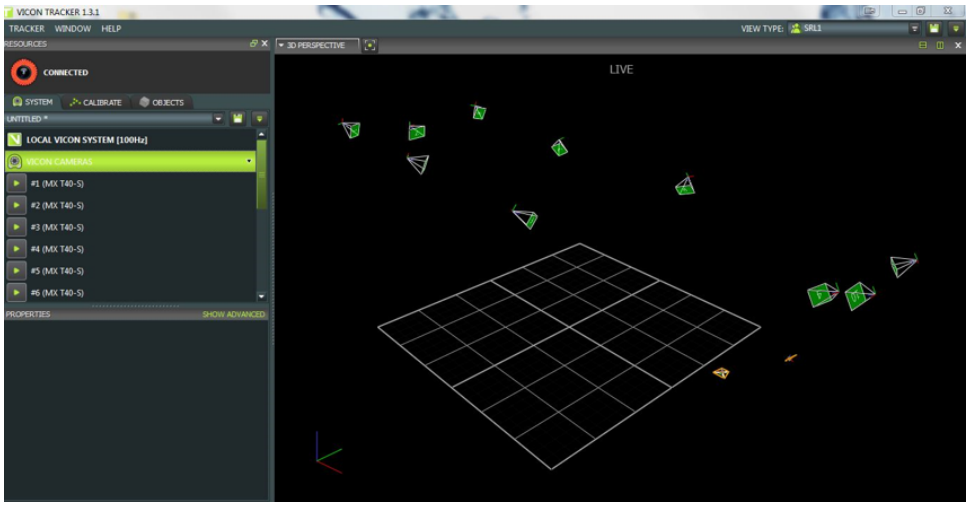

Fig. 3. VICON system at NPS laboratory

3. IDENTIFICATION OF THE HEXACOPTER

The identification of multirotors systems is usually carried out with two different approaches. One is based on the identification of physical parameters and the second is based on the variation of contol inputs and is called direct approach. Both ways are model - dipendent approaches, even if once performed on one system it can easily be repeated on other systems. The most tested approach is the idenification of physical parameters, such as moments of inertia and the relation between propeller thrust/torque and propeller angular speed. This approach was tried by [3, 29]. The other approach is the black box identification between the virtual control input and the angular rate. The second approach was tried by [2, 23]. The drawback of this second approach is that to perform the flight experiments to acquire identification data, the multirotor has to have a working controller, this means that the input signal will not be the one actually controlling the multirotor, but a reference signal to the control system or an overlay on the controller output.

For the implementation of the selected controller an open loop identification method is chosen, that is identification of physical parameters. The novelty of the proposed approach is the use of VICON system for measuring the moments of inertia and for evaluating the static gains of the engine (both thrust and torque gains). The second approach is chosen for reducing the time of collecting data and to avoid the risk of accidents during flight tests, considering that a stable and robust controller is not yet implemented on-board.

Note that for the controller chosen for this research (an $\mathcal{L}_1$ adaptive contoller) we have to evaluate a state predictor dynamics (see Section 5), thus the nominal linear model of the system should be known to obtain better performance

during flight tests and when uncertainties (i.e. variations of the flight conditions, of the system and payload masses, etc.) occur on the system.

3.1 Identification of Moments of Inertia

For the evaluation of the moments of inertia of a body usually masses and spatial distributions of the components are measured. All the distances have to be measured and all the components have to be weighted. One problem of the geometric evaluation of the moments of inertia is that the body has to be assembled or disassembled in the laboratory. If a commercial multirotor is considered (as in our case), disassembling the overall system should be time consuming.

In our case the idea is to use the rules of compound pendulum [27] for evaluating the moments of inertia of the body. It is also a prototypical system for demonstrating the Lagrangian and Hamiltonian approaches to dynamics and the machinery of nonlinear dynamics.

We assume that the moments of inertia along the X_B axis is equal to the moments of inertia of the Y_B axis, considering the mass distribution of the hexacopter.

The equations of motion are derived by Lagrangian dynamics

$$\mathcal{L} = K - V$$

where K is the kinetic energy and V is the potential energy of the pendulum. We assume that the total energy at the zero time $E(t_0)$ is equal to the maximum potential energy $V(t_0)$ and that the kinetic energy is zero. At the time t_0 we have

$$E(t_0) = -V(t_0) = -mg\cos\theta_0 l_1$$
$$K(t_0) = 0$$

where m is the total mass of the hexacopter, θ_0 is the zero inclination angle (when the potential energy is maximum), l_1 is the arm of the pendulum with respect to the pendulum CoG (distance between the yellow bar and the red point in Figure 4). The mass and geometry of the system are known. The variation of the angle θ (inclination of the pendulum, see Figure 4) is known at each time step and evaluated with the VICON system.

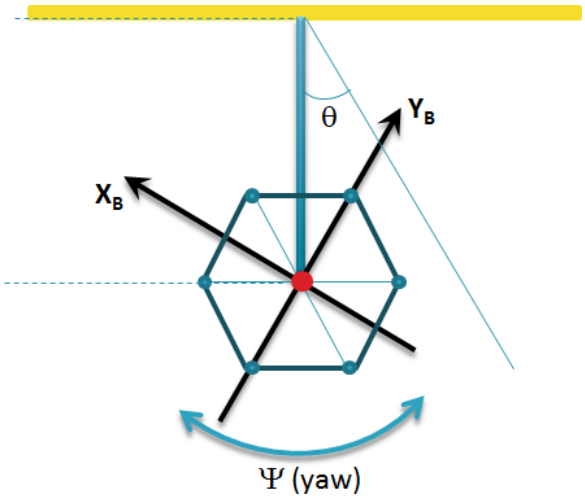

Fig. 4. Compound pendulum setup for the evaluation of the yaw moments of inertia

In the analyzed case, we have

$$V = -mg\cos\theta l_1 \quad (1)$$
$$K = \tfrac{1}{2}ml_1^2\dot{\theta}^2 + \tfrac{1}{2}I\dot{\theta}^2 \quad (2)$$

where θ is the pendulum inclination angle measured by VICON, I is the moment of inertia (unknown), $\dot{\theta} = \frac{d\theta}{dt}$ is the variation of the inclination angle with respect to time (measured by VICON). As in Eq. 2 for the pendulum rules the kinetic energy is sum of a linear and a rotational component. The unknown moments of inertia that are directly evaluated with VICON system and with the pendulum theory are the moments around the Z_B (left of Figure 5) and Y_B (right of Figure 5) axes. As in Fig. 5 the setup of the experiments is the following:

- a rigid rod is connected to the hexacopter by a system of screws and nuts,
- the same rod is connected to a structure with a base on ground.

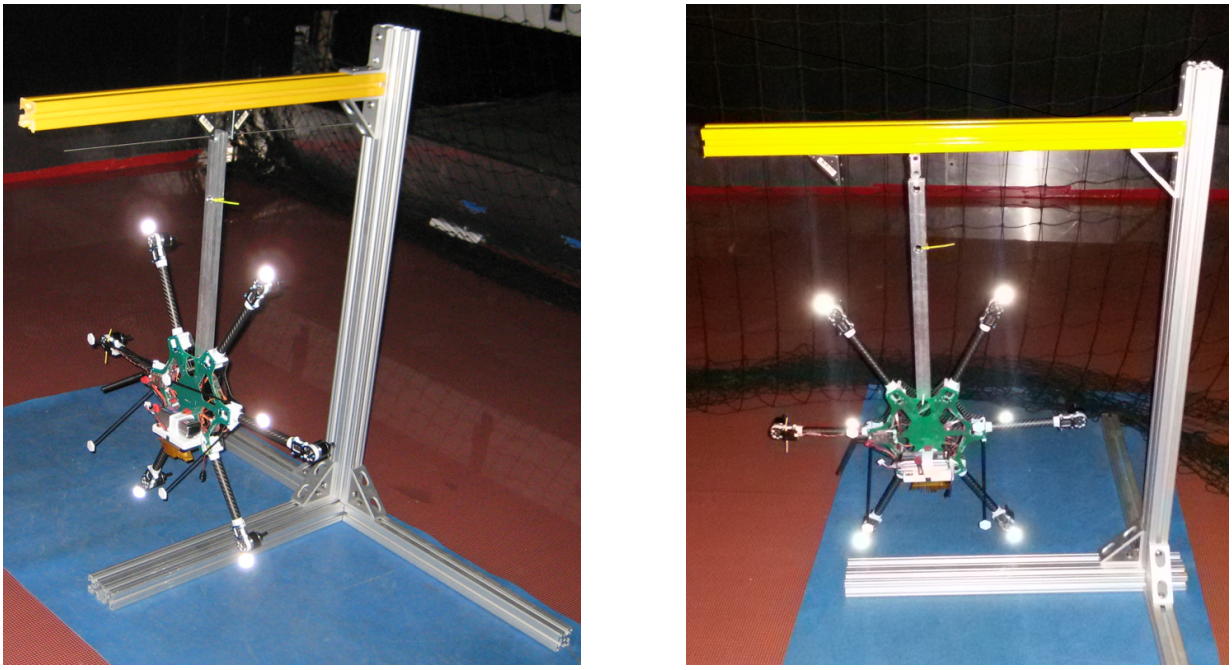

Fig. 5. Pendulum experimental setup for the evaluation of the yaw moments of inertia (left) and of the pitch moments of inertia (right)

An hexacopter object is created on VICON. Usually the zero position of the object should be setted when the platform is on the ground but, in the analyzed case, the zero angles are evaluated when the hexacopter is in the zero pendulum position (Fig. 7).

Four experiments are performed for each axes. For both moments of inertia the reference axis for the VICON measures is the X one, due to the acquisition of the zero positions. This means that the variations of the ϕ angle has to be considered. The variations of the Euler angles is in Figures 6. Not null variations of the angles along Y and Z axes is observed: (i) for the θ angle the variation is of magnitude order of 10^{-3} deg and (ii) for the ψ angle the variation is constant.

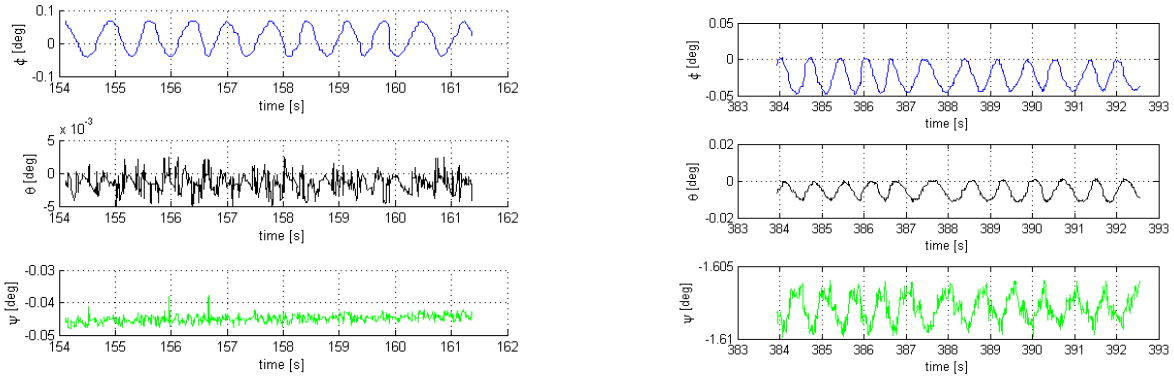

Fig. 6. Results obtained by VICON measures of pendulum inclination for the yaw moments of inertia (left) and for the pitch moments of inertia (right)

In both cases, a polynomial interpolation of the VICON data is proposed, to know at each time step the time history of the pendulum inclination angle. If the time history is known in polynomial form, the time derivative $\dot{\theta} = \frac{d\theta}{dt}$ has a straightforward expression and it could be easily evaluated. A second order polynominal approximation is proposed in the form

$$\theta(t) = a_1 t^2 + a_2 t + a_3$$

and the time derivative is

$$\frac{d\theta}{dt}(t) = 2a_1 t + a_2$$

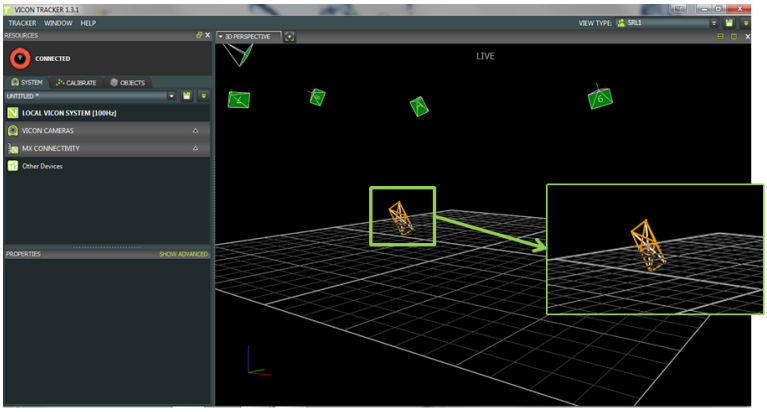

Fig. 7. Object and zero position of the hexacopter on VICON

where a_1, a_2 and a_3 are the polynomial coefficient. This approximation is applied to both moments of inertia. In that way, the only unknown variable of Eq. 2 is the moment of inertia.

$$I_{zz} = \frac{2K}{\dot{\theta}_{zz}^2} - ml_1^2$$
$$I_{yy} = \frac{2K}{\dot{\theta}_{yy}^2} - ml_1^2$$

where θ_{zz} and θ_{yy} are evaluated from Fig. 9.

For the validation of the obatined results the Lagrangian approach is applied to the pendulum. The setup of the experiments is in Fig. 8.

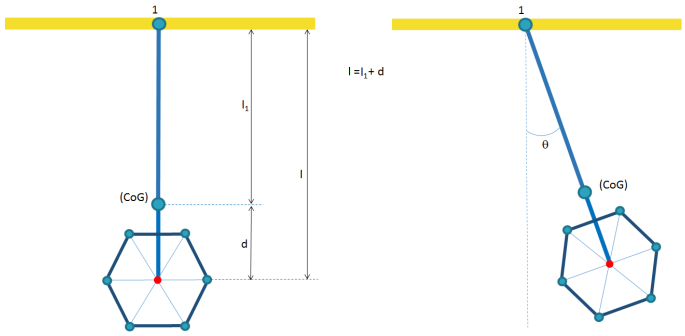

Fig. 8. Setup for the Lagrangian approach

The kinetic and potential energy can be defined as follows

$$K = \tfrac{1}{2}(m\tfrac{l_1^2}{4} + m_1(l_1 + d)^2 + I_{rod} + I)\dot{\theta}^2$$
$$V = mg(1 - \tfrac{l_1}{2}\cos\theta) + m_1 g(1 - (l_1 + d)\cos\theta)$$

where l_1 is the distance between the joint point of the rod and the hexacopter and the yellow bar, d is the distance between the joint point and the CoG of the hexacopter, m is the hexacopter mass, m_1 is the rod mass and θ is the pendulum inclination angle. I_{rod} is the moment of inertia of the bar, that is easily evaluated from the rules of parallelepiped inertia, starting from the known data of weight and geometry. I is the hexacopter moment of inertia, that is unknown. The angle θ, as in the previously cases, is evaluated by VICON. Applying the Lagrangian equation,

$$\frac{d}{dt}(\frac{\partial K}{\partial \dot{\theta}}) + \frac{\partial V}{\partial \theta} = 0,$$

with $\frac{\partial K}{\partial \dot{\theta}} = A\dot{\theta}$ and $\frac{\partial V}{\partial \theta} = B\sin\theta$.

For small angle of inclination, the natural frequancy of oscillation can be evaluated as

$$\omega^2 = \frac{B}{A}$$

where ω is the natural frequency.

From VICON experiments, the period of oscillation of the pendulum is known and can be easily evaluated from the analysis of the time history. So, we can validate at least two moments of inertia. The time histories are in Figure 9. The period of oscillation for the yaw angle (I_{zz} evaluation) is $T_z = 1.4260$ s and for the pitch angle (I_{yy} evaluation) is $T_y = 1.3909$ s.

In detail, we have

$$T_{hexa} = \frac{2\pi}{\omega} = \frac{2\pi}{\sqrt{\frac{B}{A}}}, \tag{3}$$

with T_{hexa} period of oscillation, and

$$I = \frac{T^2}{4\pi^2}(mg\tfrac{l_1}{2} + m_1 g(l_1 + d)) - m\tfrac{l_1^2}{4} + \tag{4}$$

$$-m_1(l_1 + d)^2 - I_{rod}. \tag{5}$$

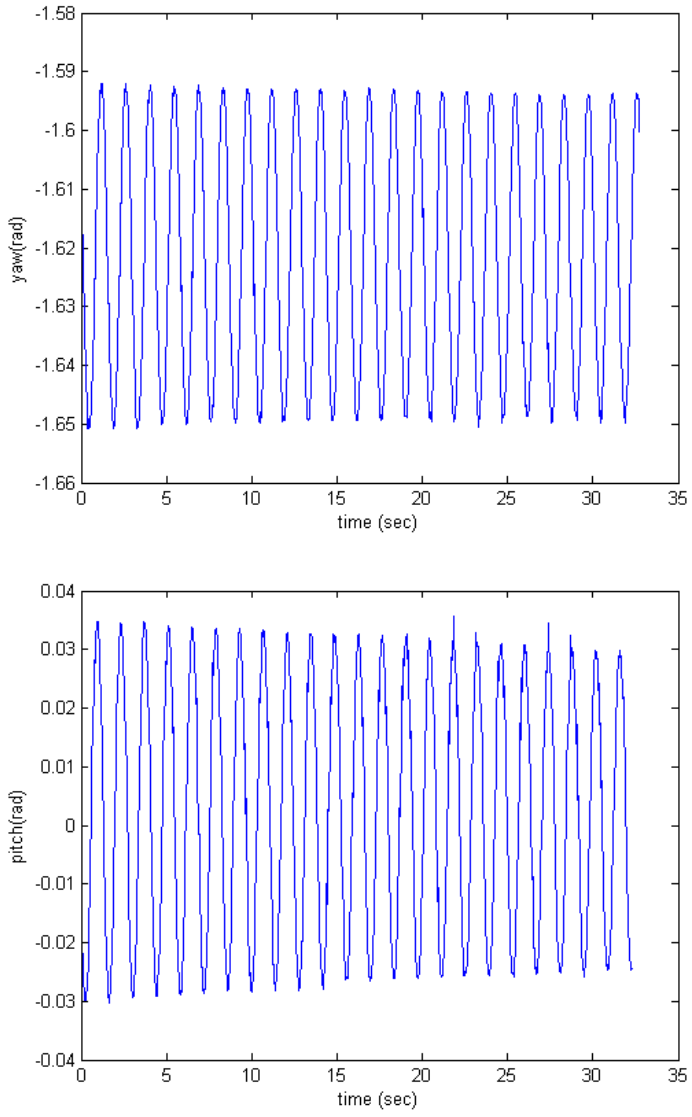

Fig. 9. Time histories of the yaw and pitch angles

The results obtained with the two experiments are very similar, as in Table 3.

3.2 Engine Identification

The thrust and aerodynamic torque produced by a propeller can be related to the rotational speed of the propeller blades. The problem is that no direct relationship between the motor input signal and the propeller angular speed

Table 2. Moments of inertia of the aluminium rod

I_{rod_x}	0.0071 kgm^2
I_{rod_y}	$2.948 \cdot 10^{-5}$ kgm^2
I_{rod_z}	0.0071 kgm^2

Table 3. Comparison between the moments of Inertia obtained with both methods

Moments of inertia	Pendulum Approach	Lagrangian Approach
I_{yy}	0.0497 kgm^2	0.0573 kgm^2
I_{zz}	0.0895 kgm^2	0.0837 kgm^2

exists. The main idea of the identification of the engine is to derive a simplified relation of the thrust generation model as in [4]. If the rotational speed of propeller i is denoted Ω_i, then the generated thrust T_i is

$$T_i = k_T \Omega_i^2 \tag{6}$$

where k_T is a propeller specific constant. In the same way, the aerodynamic torque C_i of propeller i becomes

$$C_i = k_Q \Omega_i^2 \tag{7}$$

where k_Q is a propeller specific constant for torque experiments.

The thrust constant k_T defines the relationship between the steady state thrust generated by the engines when hovering and by the angular velocity of the rotors. The hexacopter is fixed to a solid bar as a pendulum (see Fig. 10) and only one propeller is mounted.

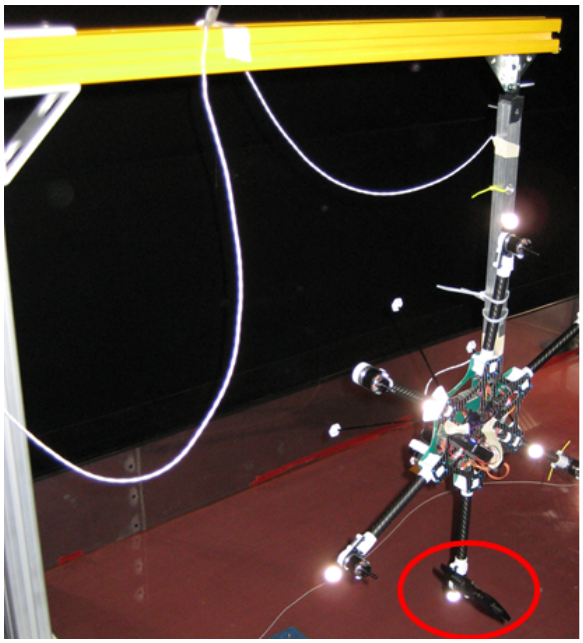

Fig. 10. Setup for the thrust experiments

As in Fig. 11, the thrust is obtained from the following equilibrium of moments around the point 1

$$m_r l_r g \sin\theta + mg \sin\theta l_2 - Tl = 0,$$

where m_r is the rod mass, l_r is the distance beween the point 1 and the CoG of the rod, m is the hexacopter total mass, l_2 is the distance between the point 1 and the hexacopter CoG, l is the distance between the point 1 and the application point of the thrust, and T is the thrust of the single engine.

Different experiments are performed at different rotational speed of the engine, in that way an analytical relationship between the thrust T and the rotational speed in PWM can be derived.

As explained before, the input signal is in PWM and it is generated by the PixHawk with a limited boundary from 1000 s to 2000 s. Motors have no response in case of PWM values smaller than the lower limit. On the other hand, a saturation phenomenon occurs for values larger than the upper limit of PWM. The experimental data are reported in Table 4. The value of thrust is related to a single engine. The idle value of PWM is 1169 s, when the hexacopter is on ground with the engines switched on. The maximum value of PWM is 1803 s, that corresponds to about 4.7 N for each engine. After this value, no significant variation of the thrust value can be observed.

An example of the experiments is in Figure 12, both VICON and PWM measures are considered. The VICON measure is related to the inclination angle (θ) of the pendulum when the hexacopter is in the configuration of Fig. 11. The PWM

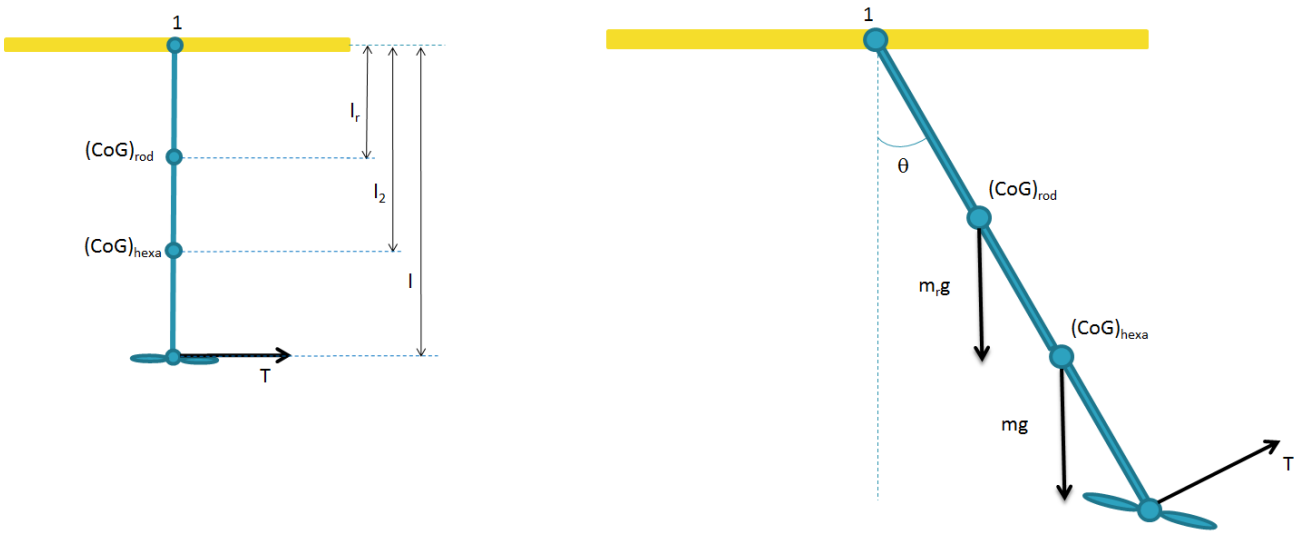

Fig. 11. Scheme for the thrust experiments

measure is the output of the PixHawk autopilot. During flight test experiments we have verified that the hovering condition is at about 1500 PWM, that is about 2.14 N for each motors (= 12.8 N for the overall configuration).

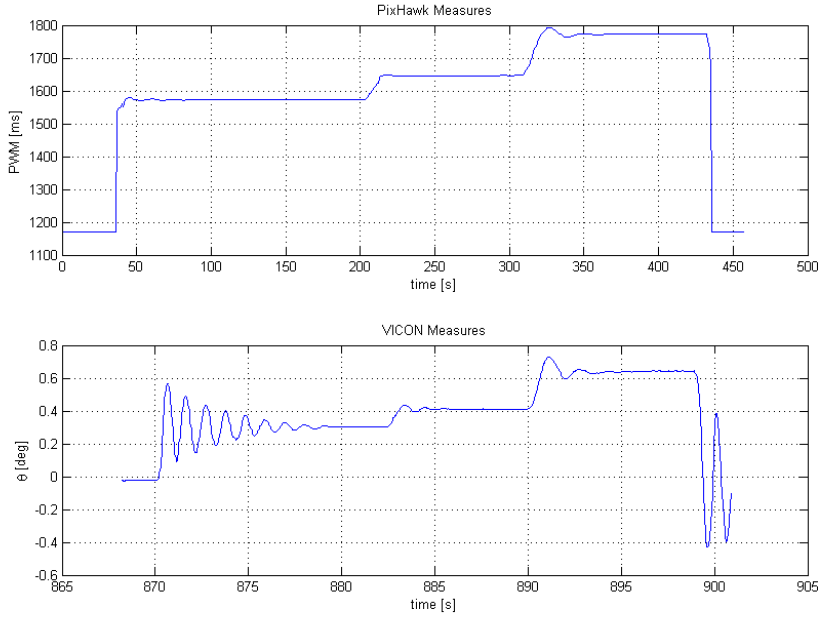

Fig. 12. Example of the results obtained with VICON and PixHawk measures

Table 4. Experimental data for thrust identification

PWM [s]	Thrust [N]
1169	0
1574	2.2119
1646	2.9366
1657	3.0123
1775	4.2924
1803	4.6627

The final relationship between PWM and thrust is

$$T[N] = 0.0071 \cdot PWM[s] - 8.5806,$$

considering a linear interpolation between the experimental data. The obtained curve is in Fig. 13. The thrust constant k_T as in Eq. 6 is equal to $1.2736 \cdot 10^{-7}$ Ns^2.

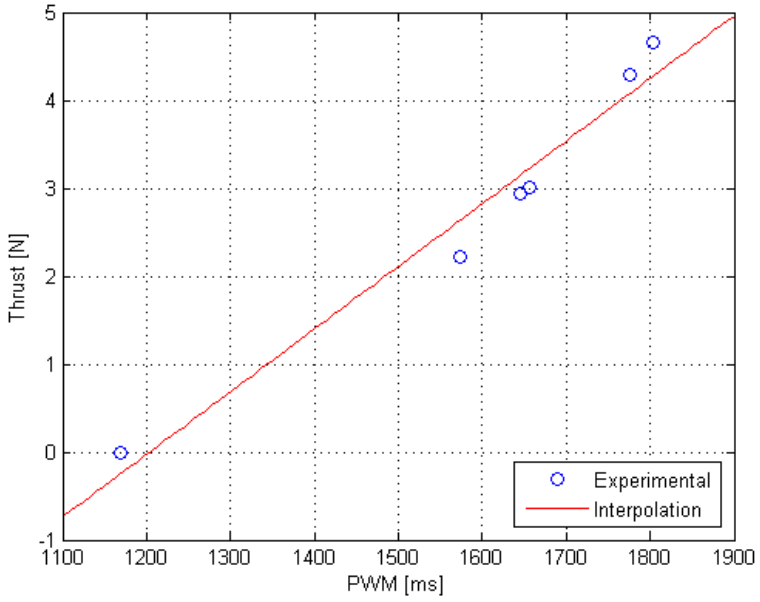

Fig. 13. Thrust variation with respect to PWM measures

The torque constant k_Q relates the rotational speed of each rotors in idle position to the torque produced by the rotor with respect to the motor axis. To find an estimate of this constant, we use a frictioless system based on experiments performed on a granite rig with floating spacecraft. See Figure 15 for the experiment setup. The hexarotor is mounted on a spacecraft that was developed at the NPS laboratory of Prof. Romano [9] and the facilities used for the experiments are on the NPS Robotics Spacelab of Prof. Romano [19] (Fig. 14).

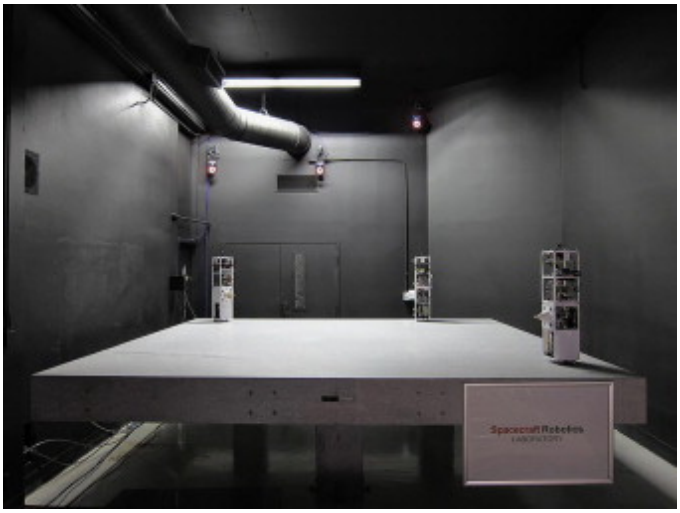

Fig. 14. The Floating Spacecraft-Simulator Testbed at Spacecraft Robotics Laboratory (NPS)

The main floating surface is a granite monolith with the following characteristics:

- Dimensions: 4 m x 4 m x 0.3 m
- Surface precision grade: AAA
- Planar accuracy:$\pm 0.127x10^{-2}$ mm
- Horizontal leveling precision: $\leq$ 0.01 deg
- Mass: 15.2 x 103 kg .

The testbed is also provided with:

- Linux Real-Time work station
- Ad-Hoc WiFi internal network for data streaming
- High pressure air compressor and compressed air filling station.

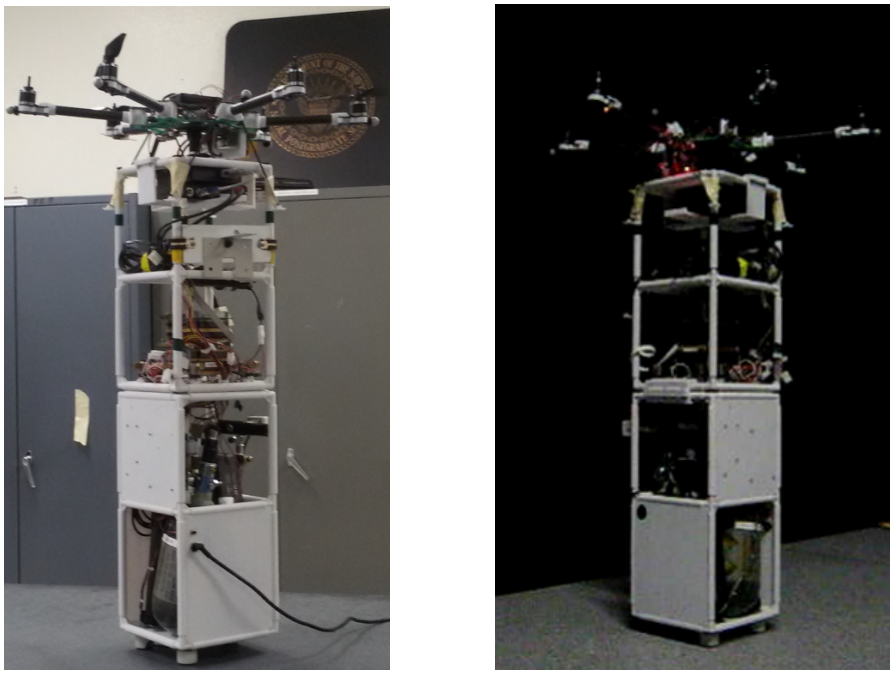

Fig. 15. Testbed setup for torque experiments

Three propellers rotating in the same direction are mounted on the hexacopter. The spacecraft is floating on the granite rig with four thrusters on. Two experiments are performed:

(1) no propellers switched on and four thrusters switched on for 5 seconds,
(2) three propellers and four thrusters switched on.

The torque is assumed to be constant for all the experiments with propellers switched off. The VICON measures with no propellers are in Fig. 16.

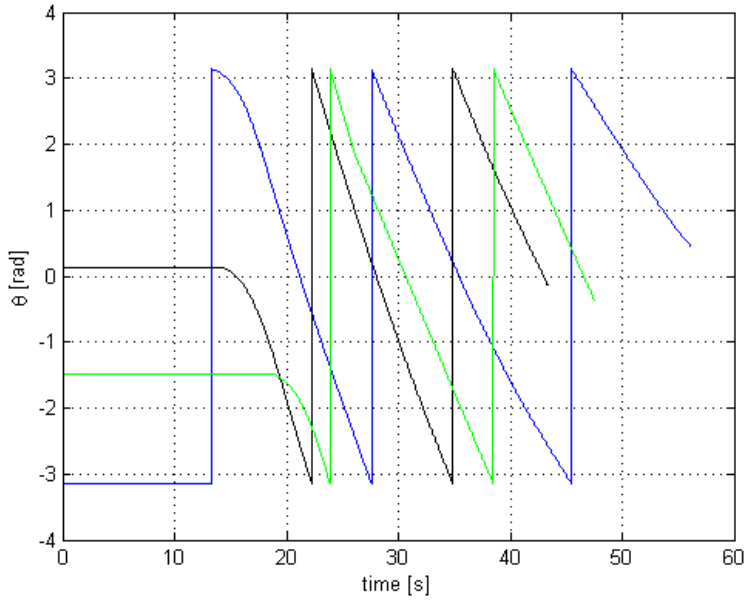

Fig. 16. VICON measures for experiment 1 (no propellers switched on)

In general, the torque τ is measured starting from the Newton's second law

$$\tau = I\dot{\omega}_{prop}, \tag{8}$$

with I moment of inertia along the Z_B of the system of Fig. 15, that means the spacecraft and the hexacopter moments of inertia and $\dot{\omega}_{prop}$ is the angular rotational speed of the body. The experiments with the propellers off are performed for the evaluation of the moment of inertia of the body I, because the torque is constant and equal to

$$\tau_0 = 2dF$$

where τ_0 is the measured torque with the propellers off, d is the distance between two thrusters and $F = 0.15$ N is the force produced by the four thrusters. In our case, τ_0 is equal to 0.0030 Nm.

Table 5. Experimental data for torque identification

PWM [s]	Torque [Nm]
1169	0.0248
1203	0.0313
1310	0.0388
1520	0.0603
1844	0.0715

The final relationship between PWM and torque

$$\tau[Nm] = 0.0001 \cdot PWM[s] - 0.0520,$$

considering a linear interpolation between the experimental data. The obtained curve is in Fig. 17. The thrust constant k_Q (as in Eq. 7) is equal to $2.4325 \cdot 10^{-9}$ Nms^2.

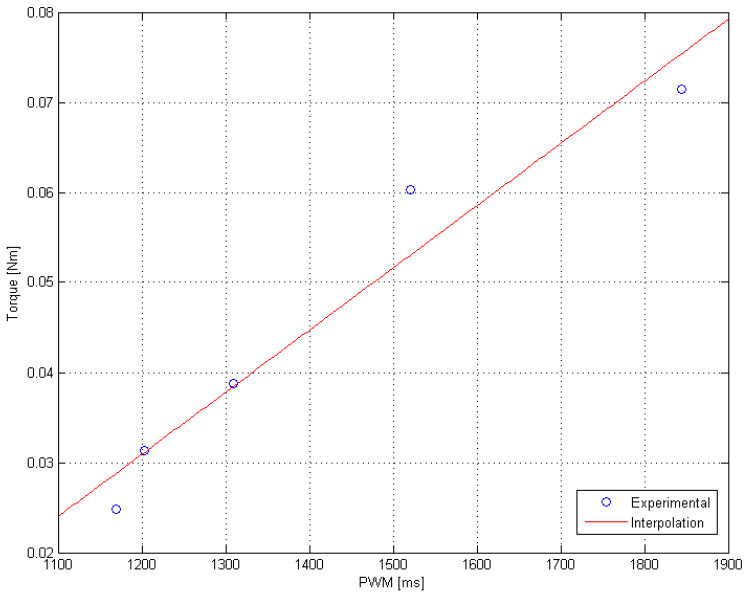

Fig. 17. Torque variation with respect to PWM measures

For the implementation of the controller, the relationship between the rotational speed of each rotor in Revolutions Per Minute (RPM) and in PWM is needed. For this reason, we use some experimental data (previously collected by NPS group), data obtained by static engine tests with the engine unmounted from its arm. The experimental data are in Fig.18. The data are ridundant for each rotational speed due to the rules of the actuator disk theory [21]. This relationship is used for the transformation between the output of the $\mathcal{L}_1$ controller (see Section 5) and the inputs of the nonlinear model implemented in Matlab (see Section 7), not only for the thrust evaluation but also for the torque evaluation. The final relationship (see Fig. 19) is

$$PWM[s] = 0.1975 \cdot RPM[rad \setminus s] + 670.0442.$$

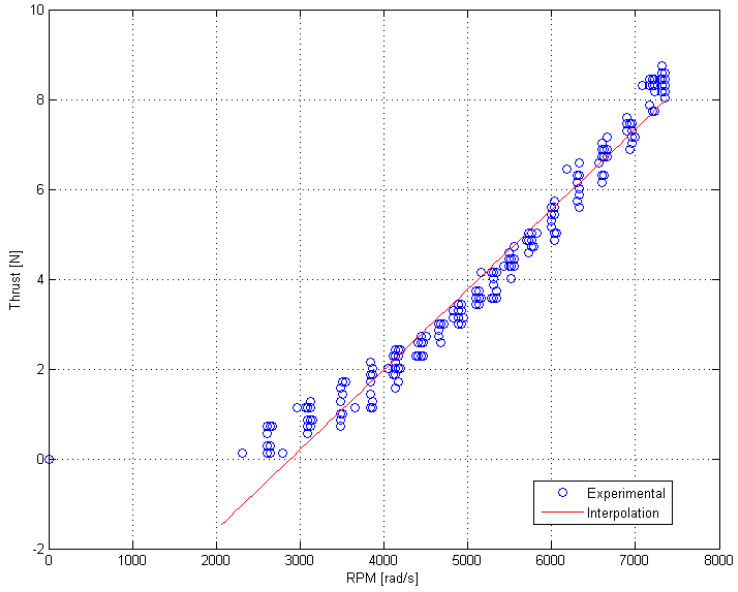

Fig. 18. Thrust vatiation with respect to RPM measures (static tests)

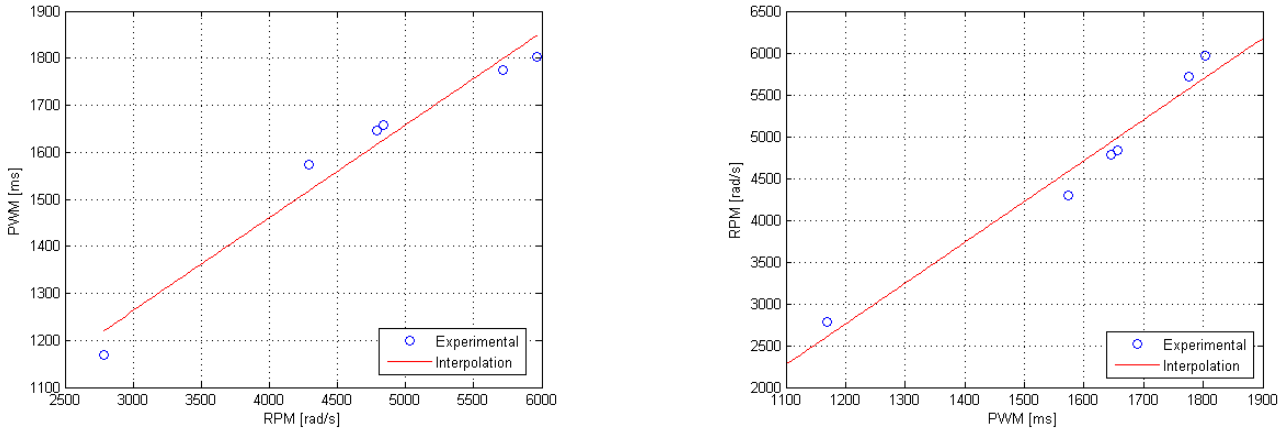

Fig. 19. Relationship between RPM and PWM measures, and viceversa

4. NONLINEAR AND LINEAR MODELS

The motion of a rigid body can be decomposed into the translational and rotational components. In order to describe the dynamics of the hexacopter, assumed to be a rigid body, the Newton-Euler equations [14] are taken into account. Nine equations of motion are considered: (i) three equations for the linear speeds with components $(u, v, w)^T$, (ii) three angular speeds $(p, q, r)^T$ and (iii) three angles $(\phi, \vartheta, \psi)^T$ for the orientation. For the linear and angular speeds, we have

$$F_B = m\frac{dV}{dt} + \omega_B \times V \tag{9}$$

$$M_B = I\dot{\omega_B} + \omega_B \times (I\omega_B) + I_p\omega_B \times ((-1)^i)\Omega_i, \tag{10}$$

where $F_B \in \mathbb{R}^3$ and $M_B \in \mathbb{R}^3$ are the total forces and moments acting on the hexacopter, respectively, m is the hexacopter total mass, $V = (u, v, w)^T \in \mathbb{R}^3$ is the vector of linear speeds, $\omega_B = (p, q, r)^T) \in \mathbb{R}^3$ is the vector of angular speeds, $I = diag(I_{xx}, I_{yy}, I_{zz}) \in \mathbb{R}^{(3,3)}$ is the inertia matrix (diagonal due to the hexacopter symmetry) with respect to the body axes. I_p is the moment of inertia about the propeller axis and is obtained as $\frac{1}{2}m_p r^2$ with m_p and r mass and radius of the propeller. Ω_i is the rotational speed of each propellers $(i = 1, \ldots, n_p)$ with n_p number of propellers. The factor $(-1)^i$ comes from the fact that the propellers rotate in opposite directions. All quantities are expressed in the body fixed frame.

The attitude of the body is described by three Euler angles $(\phi, \vartheta, \psi)^T$, which are defined by the kinematic equations and it can be obtained integrating the following equations

$$\dot{\phi} = p + q\sin\phi\tan\vartheta + r\cos\phi\tan\vartheta \tag{11}$$

$$\dot{\vartheta} = q\cos\phi - r\sin\phi \tag{12}$$

$$\dot{\psi} = \frac{q\sin\phi}{\cos\vartheta} + \frac{r\cos\phi}{\cos\vartheta}. \tag{13}$$

The forces and torques acting on the hexacopter are gravity, aerodynamic forces, air friction aerodynamic forces and torques produced by the propellers and the gyroscopic effects from the rotation of the propellers. The torque caused by the angular acceleration of the propeller has been neglected. The air frames movement through the air will cause friction. For the hexacopter this force is small and can be neglected.

To reduce the computational time and to simplify the complete model, the aerodynamic loads are calculated expressing the equations as Taylor-series-expansion (small angles of attack considered), for different propeller angular rate. The only not negligible aerodynamic loads are acting along Z_B axis, i.e. the thrust and the reaction torque. The method presented in [15] has been used to verify that the only loads noteworthy are along Z_B axis. Subsequently, torque and force varying with rpm were measured experimentally.

In the second equation of Eq. 9, the gyroscopic torque produced by the propeller can be found due that a rotating propeller follows the rotations of the airframe. Note that for multirotors the gyroscopic terms produced by propellers are the dominant ones, this is a consequence of the high rotational speed in hovering (with respect to the gyroscopic term due to the body angular rates).

The components of the total speed V can be espressed as follows

$$\dot{u} = qw - rv + g\sin\vartheta \tag{14}$$

$$\dot{v} = pw + ru - g\cos\vartheta\sin\phi \tag{15}$$

$$\dot{w} = pv - qu - g\cos\vartheta\cos\phi - \frac{\sum_{i=1}^{n_p} T_i}{m} \tag{16}$$

and the variation of the angular speeds is expressed by the following equations

$$\dot{p} = -\frac{1}{I_{xx}}[(T_3 - T_4 - T_5 + T_6)d_1 + (T_2 - T_1)l_p + qr(I_{yy} - I_{zz}) - I_p q\Omega] \tag{17}$$

$$\dot{q} = \frac{1}{I_{yy}}[(T_3 - T_4 + T_5 - T_6)d_2 + pr(I_{zz} + -I_{xx}) + I_p p\Omega] \tag{18}$$

$$\dot{r} = \frac{1}{I_{zz}}[(C_1 + C_2 - C_3 + C_4 - C_5 - C_6) - pq(I_{xx} - I_{yy})] \tag{19}$$

where T_i for $i = 1, \ldots, n_p$ is the i^{th} motor thrust, C_i for $i = 1, \ldots, n_p$ is the i^{th} motor reaction torque and $\Omega = \sum_{i=1}^{n_p}(\pm\Omega_i)$ is the total rotational speed, d_1 is the distance between the motors $(3, 4, 5, 6)$ and the X_B axis, l_p is the distance between the motors $(1, 2)$ and the X_B axis, $d_2 = \frac{\sqrt{3}}{4}l$ is the distance between the motors $(3, 4, 5, 6)$ fand the Y_B axis.

The linear model is obtained with linearization of the complete model around an equilibrium point, that is the hovering condition. The equilibrium point is chosen to guarantee zero angular rates. The speed components of X and Y axes are zero, instead a non zero value is imposed for the vertical speed ($w = 0.2$ m/s). A pitch angle of 0.02 deg is also

considered. For the linear mathematical formulation of the dynamic system a standard continous time-invariant state space formulation is derived, as follows

$$\begin{aligned} \dot{x}(t) &= Ax(t) + Bu(t), \\ y(t) &= Cx(t),\ x(0) = x_0, \end{aligned} \tag{20}$$

where $x(t) = (u, v, w, p, q, r, \phi, \theta, \psi)^T \in \mathbb{R}^9$ is the state vector, $u(t) = (\Omega_1, \Omega_2, \Omega_3, \Omega_4, \Omega_5, \Omega_6)^T \in \mathbb{R}^6$ is the control signal, $y(t) \in \mathbb{R}^l$ is the controlled output. $A \in \mathbb{R}^{9\times 9}$ is the state matrix, $B \in \mathbb{R}^{9\times 6}$ is the control matrix, $C \in \mathbb{R}^{l\times 9}$ is the output matrix, Ω_i is the rotational speed of each motor and l is the number of outputs. For the implementation of the $\mathcal{L}_1$ adaptive controller, the state vector is reduced so we have that $\tilde{x} = (u, v, w, p, q, r)^T$. The following state matrix

$$A = \begin{bmatrix} 0 & 0 & 0 & 0 & -0.20 & 0 \\ 0 & 0 & 0 & 0.20 & 0 & 0 \\ 0 & 0 & 0 & 0 & 0 & 0 \\ 0 & 0 & 0 & -0.0001 & 0 & 0 \\ 0 & 0 & 0 & 0 & 0.0001 & 0 \\ 0 & 0 & 0 & 0 & 0 & 0 \end{bmatrix} \tag{21}$$

and control matrix

$$B = \begin{bmatrix} 0 & 0 & 0 & 0 & 0 & 0 \\ 0 & 0 & 0 & 0 & 0 & 0 \\ -k_T & -k_T & -k_T & -k_T & -k_T & -k_T \\ -c_T\frac{l}{2} & c_T\frac{l}{2} & k_T d_1 & -k_T d_1 & -k_T d_1 & k_T d_1 \\ 0 & 0 & k_T\frac{\sqrt{3}}{4}l & -c_T\frac{\sqrt{3}}{4}l & k_T\frac{\sqrt{3}}{4}l & -k_T\frac{\sqrt{3}}{4}l \\ k_Q & k_Q & -k_Q & k_Q & -k_Q & -k_Q \end{bmatrix} \tag{22}$$

are obtained, where k_T and k_Q are the engine thrust and torque gains (see Section 3.2), l is the distance between engines 1 and 2 from the CoG along Y_B axis and $d_1 = \frac{l_p}{2}$. See Fig. 2 for the details.

The obtained B matrix is not invertible, thus a change of control variables is required to avoid singularity in the controller implementation. Virtual control inputs are defined considering that each rotor causes an upwards thrust force and generates a moment with direction opposite to the direction of rotation of the corresponding rotor i. Thus, the linear system in Eq. 20 could be rewritten as

$$\begin{aligned} \dot{x}_{\mathcal{L}_1}(t) &= \tilde{A}x_{\mathcal{L}_1}(t) + \tilde{B}u_{\mathcal{L}_1}(t), \\ y(t) &= Cx_{\mathcal{L}_1}(t),\ x(0) = x_0, \end{aligned} \tag{23}$$

where $x_{\mathcal{L}_1} = (w, p, q, r)^T$ is the reduced state vector, $u_{\mathcal{L}_1} = (v_1, v_2, v_3, v_4)^T$ is the virtual input vector, that is

$$\begin{aligned} v_1 &= \sum_{i=1}^{n} k_T\Omega_i^2 \\ v_2 &= -k_T\tfrac{l}{2}(\Omega_1^2 - \Omega_2^2) + k_T d_1(\Omega_3^2 - \Omega_4^2 - \Omega_5^2 + \Omega_6^2) \\ v_3 &= k_T\tfrac{\sqrt{3}}{4}l(\Omega_3^2 - \Omega_4^2 + \Omega_5^2 - \Omega_6^2) \\ v_4 &= k_Q(\Omega_1^2 + \Omega_2^2 - \Omega_3^2 + \Omega_4^2 - \Omega_5^2 - \Omega_6^2). \end{aligned} \tag{24}$$

$\tilde{A}$ and $\tilde{B}$ are defined as

$$\tilde{A} = \begin{bmatrix} 0 & 0 & 0 & 0 \\ 0 & -0.0001 & 0 & 0 \\ 0 & 0 & 0.0001 & 0 \\ 0 & 0 & 0 & 0 \end{bmatrix}$$

$$\tilde{B} = I_4.$$

5. $\mathcal{L}_1$ ADAPTIVE CONTROLLER

The choice of the $\mathcal{L}_1$ adaptive controller for the aircraft control is motivated by the high level of uncertainty which generally characterizes UAVs. The $\mathcal{L}_1$ adaptive controller here applied, extensively described in Reference [20], takes into account unmatched uncertainties which include unmodeled dynamics and state- and time-dependent nonlinearities. The adaptive law is a piecewise constant law, as explained in [6, 34], that guarantees fast estimation, the adaptation rate can be associated with the sampling rate of the autopilot board CPU. Moreover, this adaptive algorithm guarantees bounded inputs and outputs, uniform transient response and steady-state tracking. This extension of the $\mathcal{L}_1$ controller was applied to NASA's AirSTAR ([18]) and to the Boeing X-48B ([22]). A key feature of this controller, as explained in the previous works, is that the hardware interface is executed at a lower rate (about $10 - 100$ Hz) than the control algorithm (about $100 - 1000$ Hz), therefore demanding insignificant CPU power. Thus, the computational power can be used for fast adaptation.

The above described controller is designed to control the general linear system of Equation (20) which, considering uncertainties, can be rewritten as

$$\begin{aligned} &\dot{x}(t) = A_m x(t) + B_m \omega u(t) + f(x(t), z(t), t),\ x(0) = x_0, \\ &z(t) = g_o(x_z(t), t),\ \dot{x}_z(t) = g(x_z(t), x(t), t),\ x_z(0) = x_{z0}, \\ &y(t) = Cx(t). \end{aligned} \tag{25}$$

The matrix $A_m \in \mathbb{R}^{n\times n}$ is Hurwitz and specifies the desired dynamics of the closed-loop system, $B_m \in \mathbb{R}R^{n\times m}$ and $C \in \mathbb{R}^{m\times n}$ are known constant matrices. Compared to system (20), system (25) includes $\omega \in \mathbb{R}^{m\times m}$ the unknown frequency gain matrix, $z(t)$ and $x_z(t)$ respectively the output and state vector of internal unmodeled dynamics and the unknown nonlinear functions $f(\cdot)$, $g(\cdot)$ and $g_0(\cdot)$.

Another form for the first line of system (25) is

$$\dot{x}(t) = A_m x(t) + B_m(\omega u(t) + f_1(x(t), z(t), t)) + B_{um} f_2(x(t), z(t), t),\ x(0) = x_0, \tag{26}$$

with $B_{um} \in \mathbb{R}^{n\times(n-m)}$ is constant matrix such that $B_m^T B_{um} = 0$ and the rank of $B = [B_m\, B_{um}]$ is n. The unknown nonlinear functions $f_1(\cdot)$ and $f_2(\cdot)$ satisfy the condition

$$\begin{bmatrix} f_1(x(t), z(t), t) \\ f_2(x(t), z(t), t) \end{bmatrix} = B^{-1} f(x(t), z(t), t).$$

The state predictor is defined as

$$\dot{\hat{x}}(t) = A_m \hat{x}(t) + B_m(\omega_0 u(t) + \hat{\sigma}_1(t)) + B_{um}\hat{\sigma}_2(t),\ \hat{x}(0) = x_0$$

where $\hat{\sigma}_1(t) \in R^m$ and $\hat{\sigma}_2(t) \in R^{n-m}$, with ω_0 a suitable value for ω. The adaptation laws are

$$\begin{bmatrix} \hat{\sigma}_1(t) \\ \hat{\sigma}_2(t) \end{bmatrix} = -\begin{bmatrix} \mathbb{I}_m & 0 \\ 0 & \mathbb{I}_{n-m} \end{bmatrix} B^{-1}\Phi^{-1}(T_s)\mu(iT_s), \tag{27}$$

for $i = 0, 1, 2, ...$, and $t \in [iT_s, (i+1)T_s]$, where $T_s > 0$ is the adaptation sampling time associated with the sampling rate of the CPU installed on the autopilot board. In Equation (27) also appear

$$\begin{aligned} &\Phi(T_s) = A_m^{-1}(e^{A_m T_s} - \mathbb{I}_n),\ \in R^{n\times n} \\ &\mu(iT_s) = e^{A_m T_s}\tilde{x}(iT_s), \end{aligned}$$

where $\tilde{x}(t) = \hat{x}(t) - x(t)$ is the error between the system state and the predicted state.

Finally, the last element of the controller is the control law defined as

$$u(t) = -K\chi(t).$$

Calling s the complex argument resulting from the Laplace transform of the corresponding time domain signal, it is possible to define

$$\begin{aligned} &\chi(s) = D(s)\hat{\eta}(s), \\ &\hat{\eta}(t) = \omega_0 u(t) + \hat{\eta}_1(t) + \hat{\eta}_{2m}(t) - r_g(t), \\ &\hat{\eta}_1(t) = \hat{\sigma}_1(t), \\ &\hat{\eta}_{2m}(s) = H_m^{-1}(s)H_{um}(s)\hat{\sigma}_2(s), \\ &r_g(s) = K_g(s)r(s). \end{aligned}$$

$D(s)$ is a proper stable transfer matrix of dimension $m \times m$, $r(t)$ is the reference signal. The transfer functions H_m and H_{um} are calculated starting from the matrices of systems (25) and (26)

$$\begin{aligned} &H_m(s) = C(s\mathbb{I}_n - A_m)^{-1}B_m \\ &H_{um}(s) = C(s\mathbb{I}_n - A_m)^{-1}B_{um} \end{aligned}$$

while the prefilter $K_g(s)$ is chosen as the constant matrix $K_g = -(CA_m^{-1}B_m)^{-1}$ to achieve decoupling among the signals.

The first step is to find the matrix A_m, which describes the desired closed loop dynamics. This Hurwitz matrix is found using the pole placement theory. The pole placement must be done considering the desired dynamic specifications. A robust eigenstructure is assigned taking into account that the more negative is the real part of the poles, the faster is the speed with which the system reaches its steady state. If the state feedback is designed by eigenstructure assignment, not only the eigenvalues but also the right generalized eigenvectors can be assigned [30, 32].

For the $\mathcal{L}_1$ controller is not necessary that the desired dynamics are near to the real one, as said before. The desired response is chosen considering the change of variables described in Section 4 and in Eq. 24:

- All the inputs are decoupled.
- Fast response on the pitch and roll variable
- Slow response on the variation of the vertical speed and on the yaw axis.

Usually, the variation of the vertical speed and of the yaw angle should be slower than the other dynamics for multirotors, to avoid sudden responses on Z_B. The desired step response dynamics is in Fig. 20. The blue line is the behaviour before the decoupling of the controlled variables, and the green line is the linear behaviour with decoupled input variables.

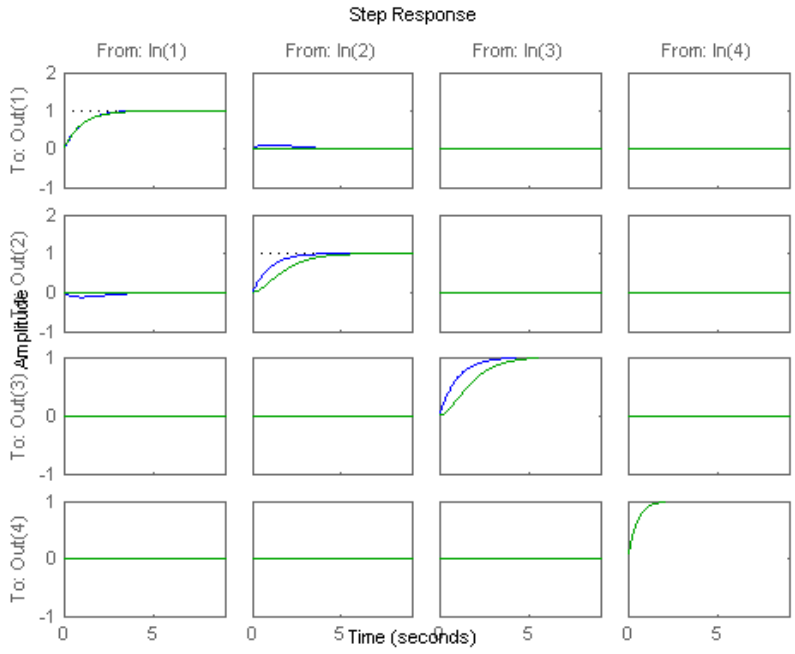

Fig. 20. Step response of the desired linear system

An important feature of the $\mathcal{L}_1$ controller is that the error between the closed loop system with the $\mathcal{L}_1$ controller and the reference controller can be uniformly bounded by a constant inverse proportional to the square root of the rate of adaptation, similar to the tracking error [20]. The selected time step is equal to $T_s = 100$ Hz, due to on-board microcontroller constraints.

Another important key aspect is that this controller defines the control signal as the output of a low pass-filter to guarantee that the control signal stays in the low-frequency range. This feature permits to avoid high frequency oscillations due to the large adaptation gain. In systems that use electric devices these oscillations significantly increase the current draw and it is undesirable. Thus, the inner loop control objective is to design a full state feedback controller for the system such that all the closed loop signals remain bounded and the system tracks the state of a desired reference model.

A model obtained from experimental flight tests can present some variations with the ideal case, but, if the controller do not require a retuning, this controller can be considered robust, due to good performance in terms of overshoot and rise time. The $\mathcal{L}_1$ controller can be implemented to limit the range of the angular velocities and of the four rotor rotational speed. Notice that a quadrotor is an unstable platform, thus, if a sudden maneuver is implemented, it can cause glitches on the parameters trend and the aircraft could become uncontrollable.

6. LINEAR QUADRATIC REGULATOR

The theory of optimal control is concerned with operating a dynamic system at minimum cost. The case where the system dynamics are described by a set of linear differential equations and the cost is described by a quadratic function is called the LQ problem. One of the main results in the theory is that the solution is provided by the linear-quadratic regulator (LQR). The results obatined with the $\mathcal{L}_1$ adaptive controller are compared with this robust controller.

Starting from state-space model (see Equation 23), the controlled output $y(t)$ corresponds to a signal that has to be small as possible in the shortest possible amount of time. In this case, the controlled output is coincident with the measured one, which corresponds to the signal that can be measured. The optimal LQR problem consists of finding the controller transfer-matrix $C(s)$ that minimizes the cost function J_{LQR} [11]. The assumption is that the whole state $x(t)$ can be measured and it is available for control.

The cost function can be defined as

$$J_{LQR} = \int_0^\infty (x'(t)Qx(t) + \rho u'(t)Ru(t))dt \tag{28}$$

where $Q \in \mathbb{R}^{n\times n}$ is a symmetric positive-definite matrix, $R \in \mathbb{R}^{n\times m}$ a symmetric positive-definite matrix, ρ is a positive constant, n is the state vector dimension and m is the input vector dimension. The optimal state-feedback controller is a simple matrix gain of the form

$$u = -Kx$$

where $K \in \mathbb{R}^{m\times n}$ is given by the following expression

$$K = \rho R^-1 B^T P(t),$$

ans $P(t)$ is found by solving the continuous time Algebraic Riccati Equation (ARE),

$$A^T P(t) + P(t)A - P(t)BR^-1B^t P(t) + Q = -\dot{P}(t).$$

The matrices Q and R are chosen using the Bryson's rule [17], that is select Q and R diagonal with

$$Q_{ii} = \frac{1}{maximumacceptablevalueofx_i^2}, i \in (1, 2, ..., n)$$
$$R_{jj} = \frac{1}{maximumacceptablevalueofu_j^2}, j \in (1, 2, ..., m)$$

which correspond to the following criteria

$$J_{LQR} = \int_0^\infty (\sum_{i=1}^{n} Q_{ii}x_i^2(t) + \rho \sum_{j=1}^{m} R_{jj}u_j^2(t))dt.$$

A crucial property of LQR controller design is that this closed-loop is asymptotically stable as long as the following two conditions hold:

(1) The system is controllable.
(2) The system is observable.

In the analyzed case, the rank of the matrix $(\tilde{A}, \tilde{B})$, that is the controllability matrix, is equal to 4. Thus the state space system in (23) is controllable. The observability is guaranteed because the output matrix C is the identity matrix.

For any bounded input $u(t)$, the output $y(t)$ and the state $x(t)$ are also bounded, i.e.

$$\|u(t)\| \leq c_1, \forall t \geq 0$$
$$\|y(t)\| \leq c_2, \forall t \geq 0$$
$$\|x(t)\| \leq c_3, \forall t \geq 0,$$

with c_1, c_2 and c_3 defined boundaries. Moreover, if $u(t)$ converges to zero as $t \to \infty$, then $x(t)$ and $y(t)$ also converge to zero as $t \to \infty$.

For the analyzed hexacopter, the control is assigned by the four virtual inputs v_i (Eq. 24) and the outputs are $y = (w, p, q, r)^T$. The LQR weights are equal to 0.6, both the state and input weight.

7. SIMULATION AND EXPERIMENTAL RESULTS

Some simulations are performded for validate the nonlinear model and for evaluate the performance of LQR and $\mathcal{L}_1$ controllers in closed loop.

In the first case, the nonlinear model implemented on Simulink and the experimental flight performed with the PixHawk are compared. Starting from the identification of the dynamic models, a complete nonlinear model is implemented in Matlab/Simulink, considering Eqs. 11-17. A Matlab function is implemented for the calculations of the thrust and torque of each engines. For the validation, the time history of the rotational speeds of the rotors has to be analyzed. Starting from the experimental flight, performed in the NPS laboratory, the inputs of the nonlinear model should be the vector of time (uniformly distributed and with a fixed sample time) and the variations of PWM (outputs of the PixHawk). In Fig.21 the command block and the Matlab function are reported. All the inputs obtained in the experimental flight have to be separetely saved and converted in rpm^2, that is the input of the nonlinear model and also the output of the $\mathcal{L}_1$ controller.

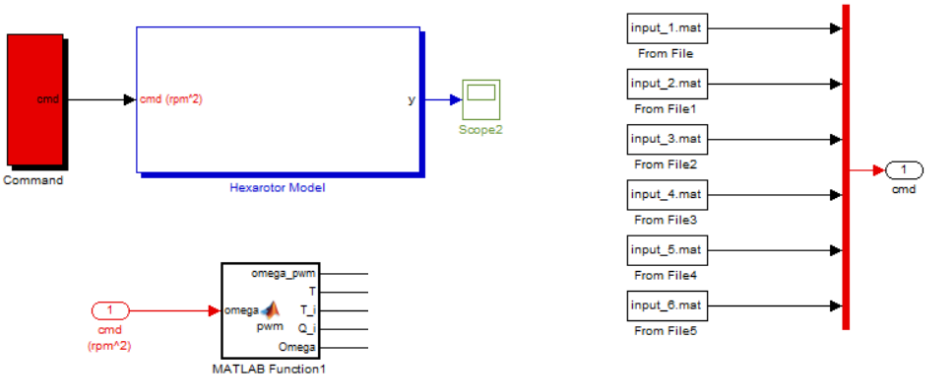

Fig. 21. Matlab model of the nonlinear system

As previously discussed, from static tests of the single engine we could define PWM-RPM and viceversa (see Fig. 19). In that case, we know the PWM variations from the PixHawk logs and we would like to evaluate the variation of the rpm, that is

$$RPM[rad \setminus s] = 0.0049 \cdot 10^3 \cdot PWM[s] - 3.0786.$$

The variations of the inputs are in Fig.22.

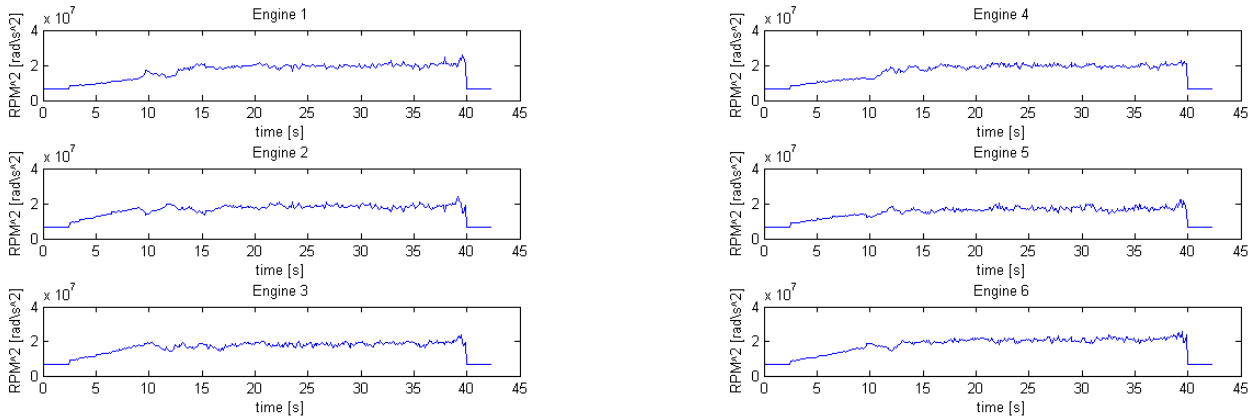

Fig. 22. Input variations from PixHawk experiments

The measured outputs from the PixHawk are the attitude angles. The compared results are in Fig. 23. Similar results are obtained for the variation of the pitch angle, instead for the roll and yaw angles the errors between the nnlinear simulated model and the real one is not neglegible. An error of about 3 deg is measured for the roll angle and of about 10 deg for the yaw angle. This is probably due to evaluation of the moments of inertia. However, due to the hihgly nonlinearity of the analyzed system the obtained results can be considered acceptable, taking into account that the scope of the project is the implementation of a feedback controller.

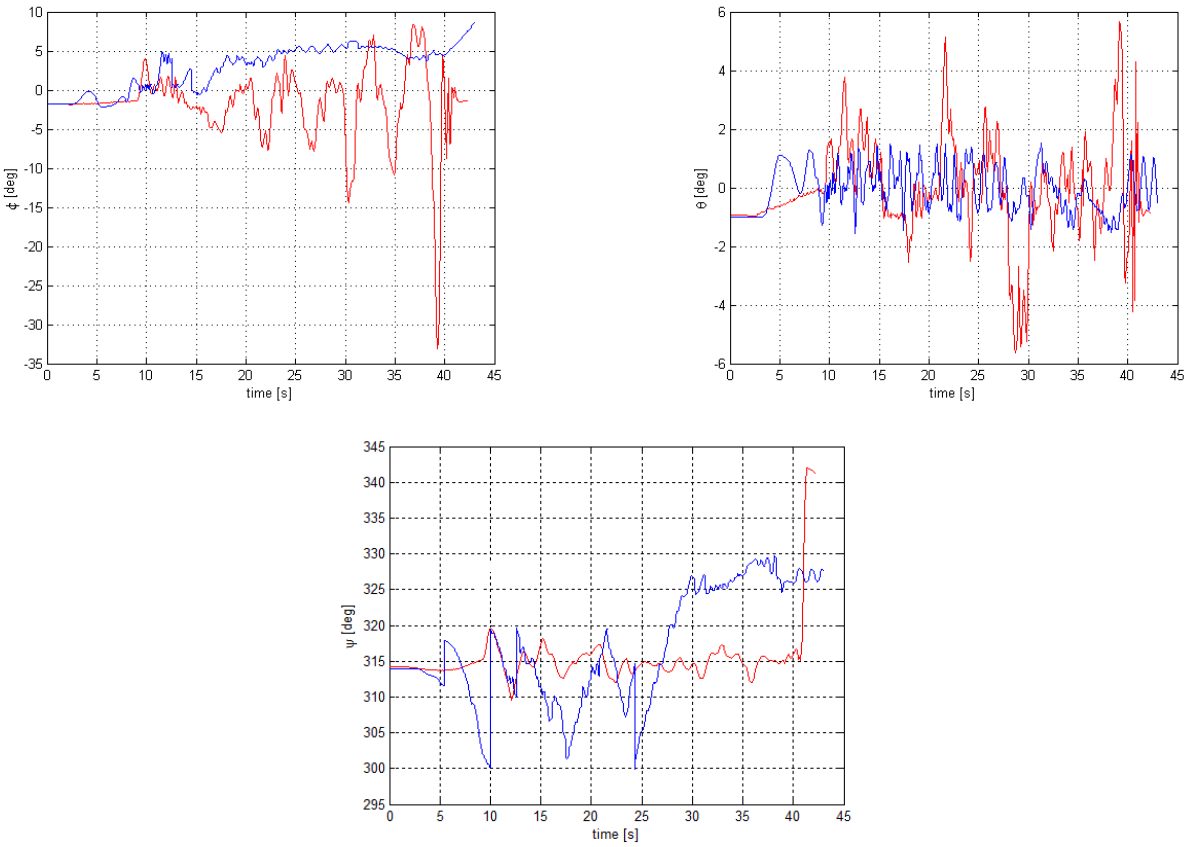

Fig. 23. Comparison between the nonlinear model and the experimental flight. Red line = Experimental flight, Blue line = Simulated Nonlinear Model

For the validation of the identification of the engine characteristics and of the implementation on Matlab/Simulink, the output of the Matlab function in Fig. 21 are also considered. The time histories of the following variables are analyzed:

(1) the variation of PWM with respect time, that has to be compared with the time histories of the experimental flight,
(2) the variation of thrust of each engine as in Eq. 6,
(3) the variation of the torque of each engine, as in Eq. 7.

As clear from Fig. 24, a correct interpolation of the data is performed in the implementation of the Matlab model. Miminum error can be obtained from the simulated input variations and the real flight inputs.

The second step is the implementation of the LQR controller and of the $\mathcal{L}_1$ controller in Matlab. See Figs. 27 and 28.

As in Fig. 27, for the implementation of both controllers, the time history definition of the variable v_i is required. As indicated in Eq. 24, the virtual inputs are function of the variation of the rotational speed (square of these variations) and of the constants related to the thrust and torque variations (Eqs. 6 and 7).

Two cases are considered for the comparison of the proposed controllers:

- ideal case
- experimental case

For the ideal case, considering the time histories of the experimental virtual inputs, we have:

(1) a step variation of about 10 N is imposed on the virtual input v_1, that is the input related to the thrust and, as consequence, related to the hovering maneuver.
(2) a doublet maneuver of 0.00087 Nm is imposed on the virtual inputs v_2 and v_3 at different time step.
(3) a step variation of about 0.00018 Nm is imposed on the virtual input v_4.

See Fig.29 for the graphical variations of the virtual inputs. These virtual inputs are transformed in variations of the rotational speeds of the six rotors using the Moore-Penrose pseudoinverse [24, 26], that is a generalization of the inverse matrix and is unique.

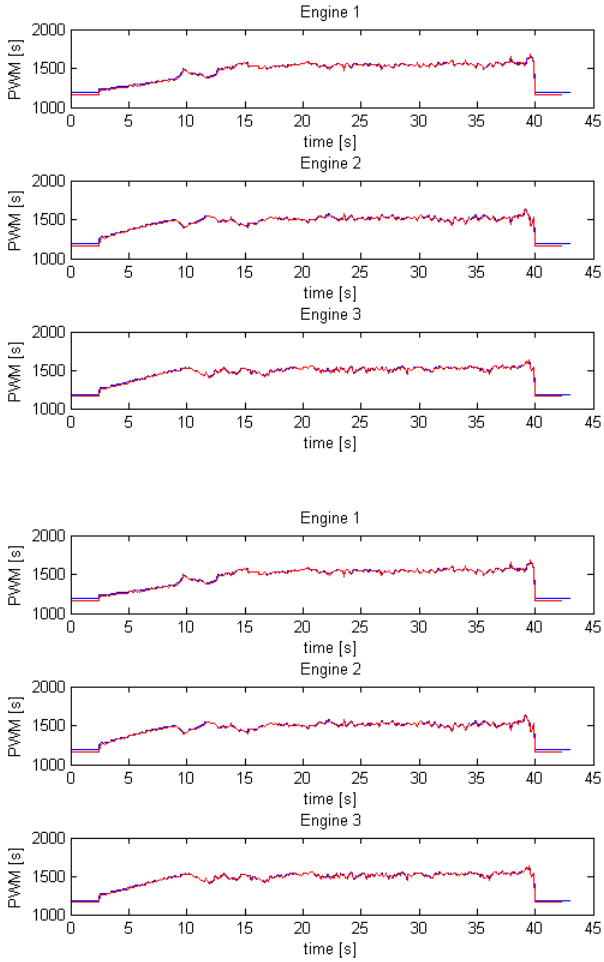

Fig. 24. Comparison between the PWM variations of the nonlinear simulated model and the experimental flight. Red line = Experimental flight, Blue line = Simulated Nonlinear Model

As in Figs. 30-33, we can observe that both controllers have good performance following ideal step variations of the input variables. The implementations of the LQR controller cannot provide any information about the sample time of the simulations and about the assigned controlled inputs. With the $\mathcal{L}_1$ adaptive controller we could observe also the variations of the controller assigned inputs. See Fig. 34.

Considering an example of flight tests, as in the previous case, the time histories of the virtual inputs are in Fig. 35. For the validation of both controllers, these inputs are considered.

The time histories of the controlled variables are in Figs. 36-39. As in the previous case, both controllers have good behaviour, even if the inputs are noised and not filtered.

The controlled $\mathcal{L}_1$ inputs are in Fig. 43. For the $\mathcal{L}_1$ adaptive controller we could also simulate the following cases:

(1) ideal inputs that include an actuator model with time delay,
(2) experimental inputs that include an actuator model with time delay,
(3) nonlinear model that include an actuator model with time delay.

In the LQR controller we cannot include an actuator model and we cannot simulate the behaviour of the nonlinear model. To validate the LQR with time delay, we have to flight with the hexacopter and upload the output time histories of the PixHawk.

A different time delay is considered for all channels:

(1) a time delay of one sample time (0.01 s) in the virtual input v_1,
(2) a time delay of 0.02 s in the virtual input v_2,
(3) a time delay of one sample time (0.01 s) in the virtual input v_3,
(4) a time delay of 0.04 s in the virtual input v_4.

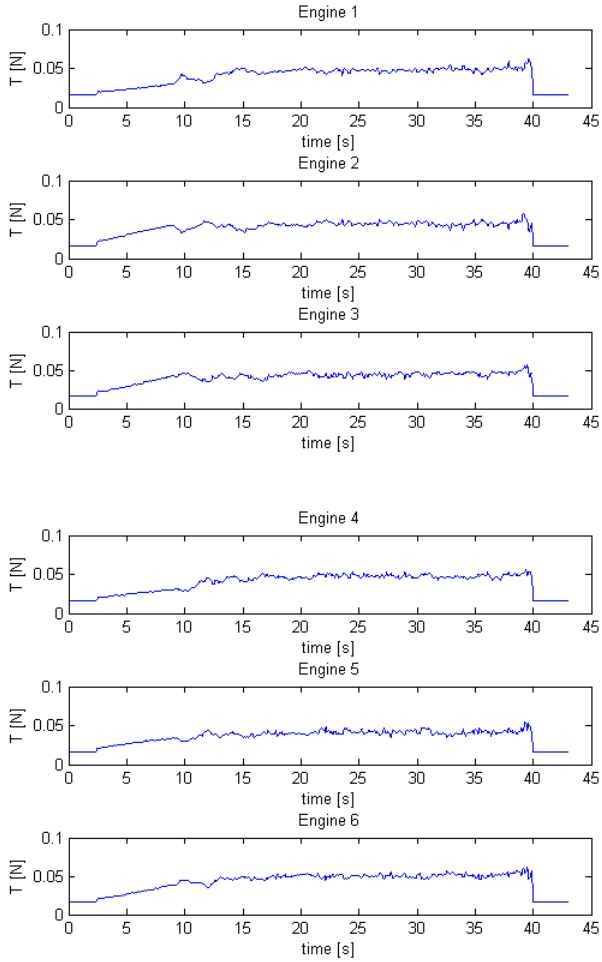

Fig. 25. Time history of the thrust variation of the six engines

A first order transfer function is considered for all channels for the simulation of the actuator model. The time delay is considered for simulate a delay in the connection between the input signal sent by Matlab UDP sender and the UDP receiver on PixHawk model. This connection is briefly described on Section 8.

The first analyzed case is related to the ideal inputs with a delay and an actuator model on the controlled input. The delay is introduced between the output of the control law and the hexacopter model. The obtained results are in Fig. 40. As visible from the obtained results, the zero value of the variables is easily reached before the end of the simulations. However, the maximum value of each variables is never reached.

The second analyzed case is related to the experimental inputs, including an actuator model with time delay. The obtained results are in Fig. 41.

The last case considered is the nonlinear model with time delay and actuator models between the controller outputs and the hexacopter model. For clearly understand the obtained results, the nonlinear model should be rewritten considering the changed of input variables. The Eqs. 14 and 17 are rewritten as

$$\dot{w} = pv - qu - g\cos\vartheta\cos\phi + \tfrac{v_1}{m} \tag{29}$$

$$\dot{p} = -\tfrac{1}{I_{xx}}[v_2 + qr(I_{yy} - I_{zz}) - I_p q\Omega] \tag{30}$$

$$\dot{q} = \tfrac{1}{I_{yy}}[v_3 + pr(I_{zz} - I_{xx}) + I_p p\Omega] \tag{31}$$

$$\dot{r} = \tfrac{1}{I_{zz}}[v_4 - pq(I_{xx} - I_{yy})]. \tag{32}$$

The inputs of the nonlinear model are the virtual inputs v_i and the outputs are $y = (w, p, q, r)^T$. In that case, in the comparison between the assigned inputs and the obtained outputs, we have to take into account that the virtual inputs are only a part of the nonlinear model. Thus, if the time history of the vertical speed w is analyzed, we can observe that this speed is not stabilized. This is due because the variation of the other linear speed components influence its behaviour, and u and v are not controlled. The time histories of all the angular speeds is coupled by the variation of

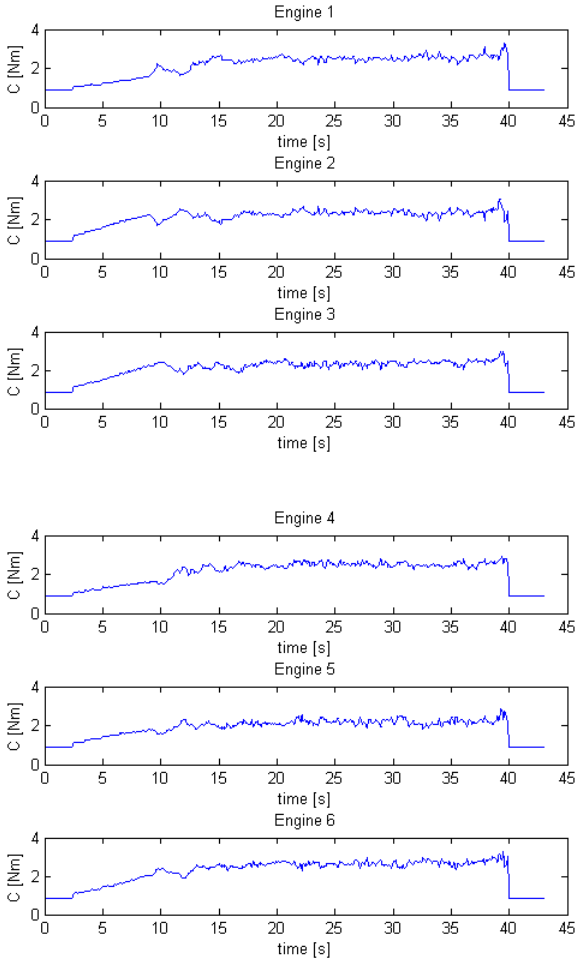

Fig. 26. Time history of the torque variation of the six engines

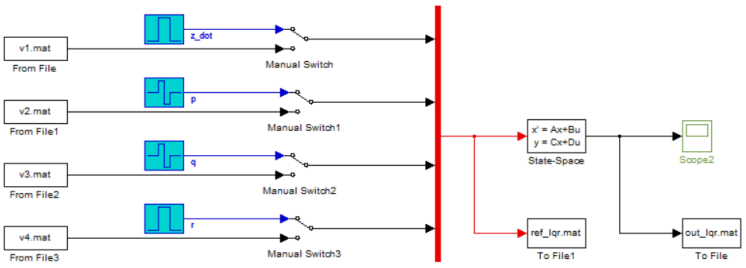

Fig. 27. Simulink file for the implementation of LQR controller

the angular speed of the other body axes. In that case, all the variables are controlled so they asymptotically converge to a reference value, that is different from zero. All the time histories are in Fig. 42. The blue line are the virtual inputs v_i obtained by the application of the experimental inputs with an $\mathcal{L}_1$ adaptive controller.

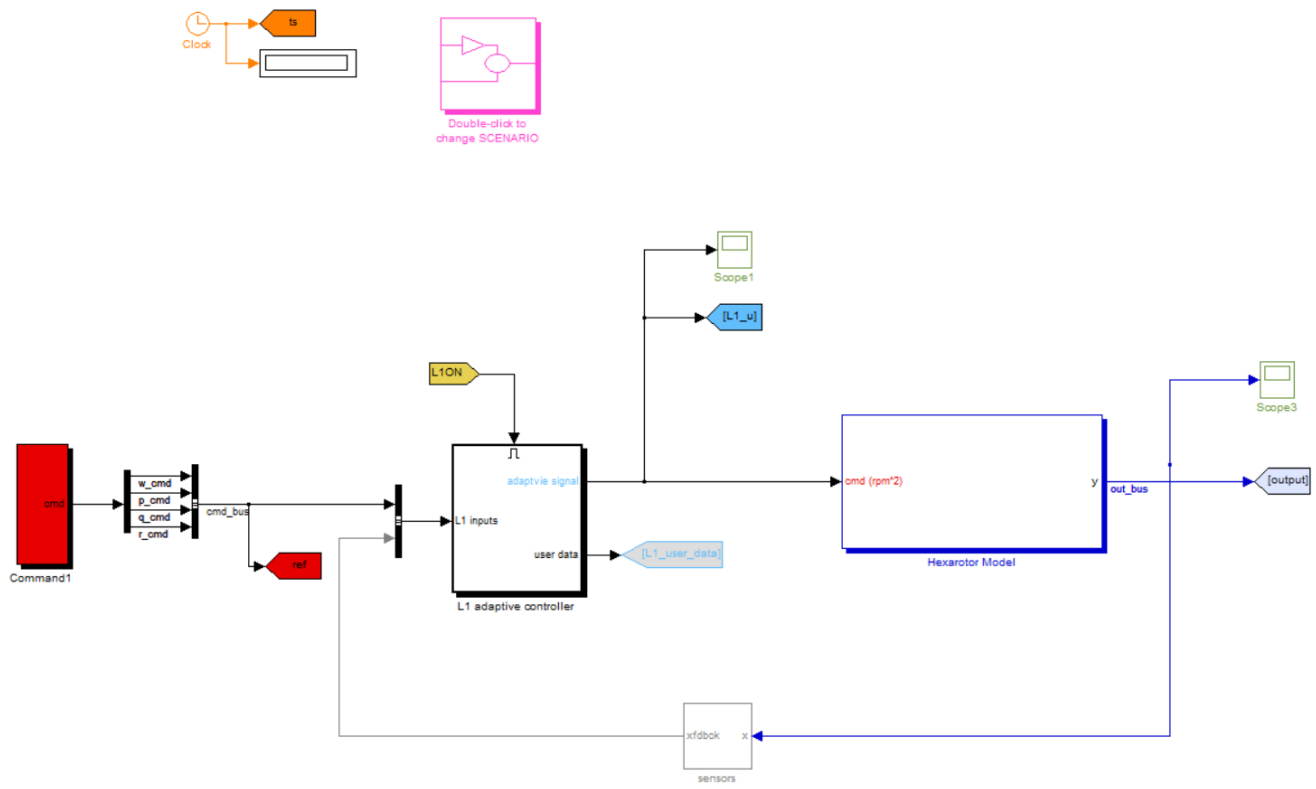

Fig. 28. Simulink file for the implementation of $\mathcal{L}_1$ controller

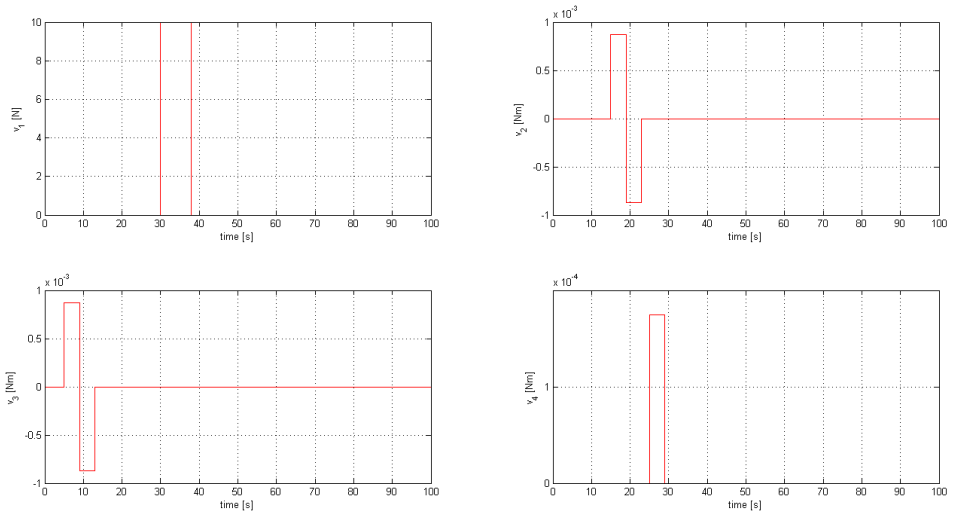

Fig. 29. Time histories of the virtual inputs for the ideal case

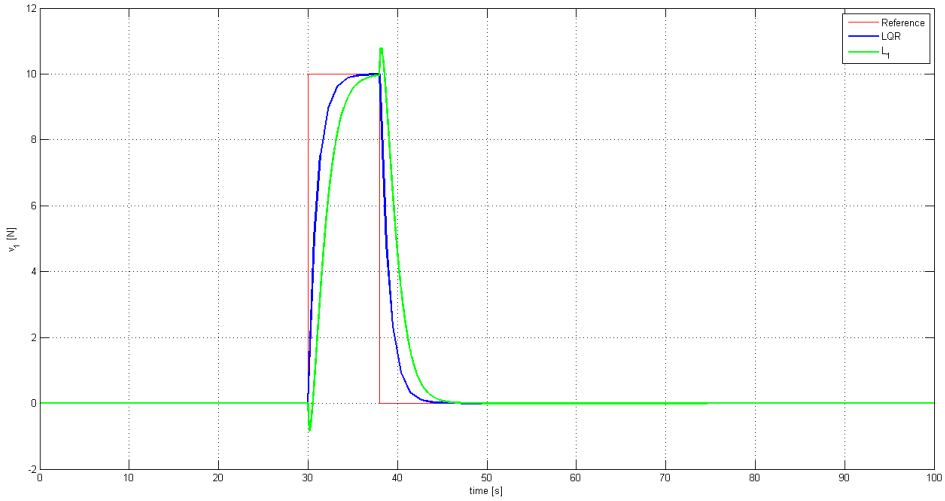

Fig. 30. Closed loop time histories of the virtual input v_1 for both controllers

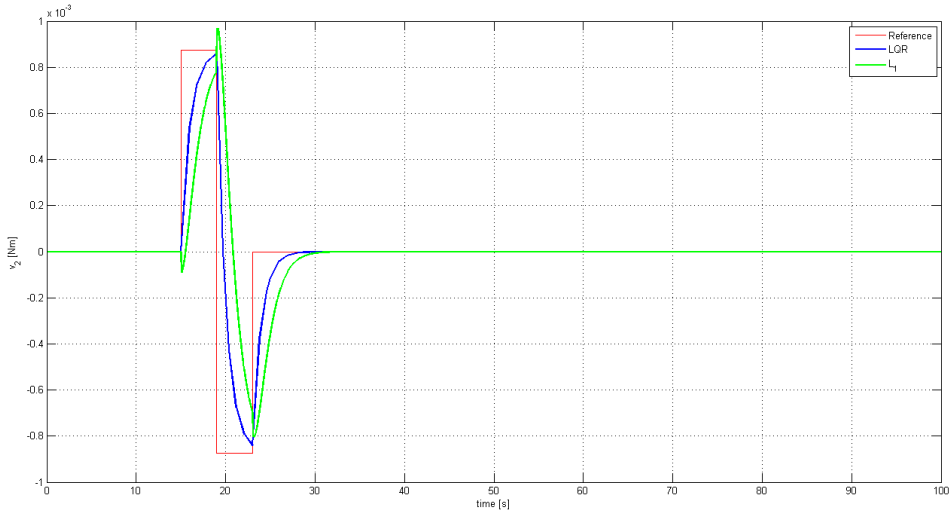

Fig. 31. Closed loop time histories of the virtual input v_2 for both controllers

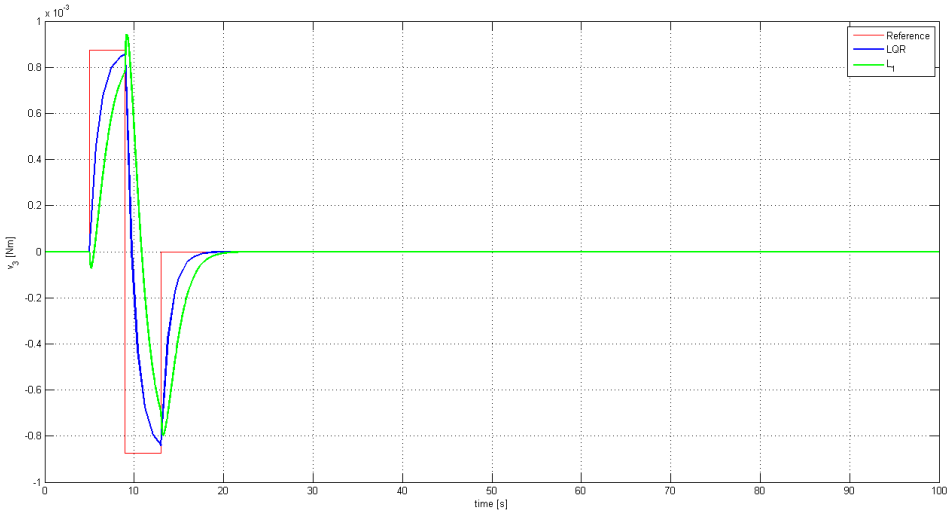

Fig. 32. Closed loop time histories of the virtual input v_3 for both controllers

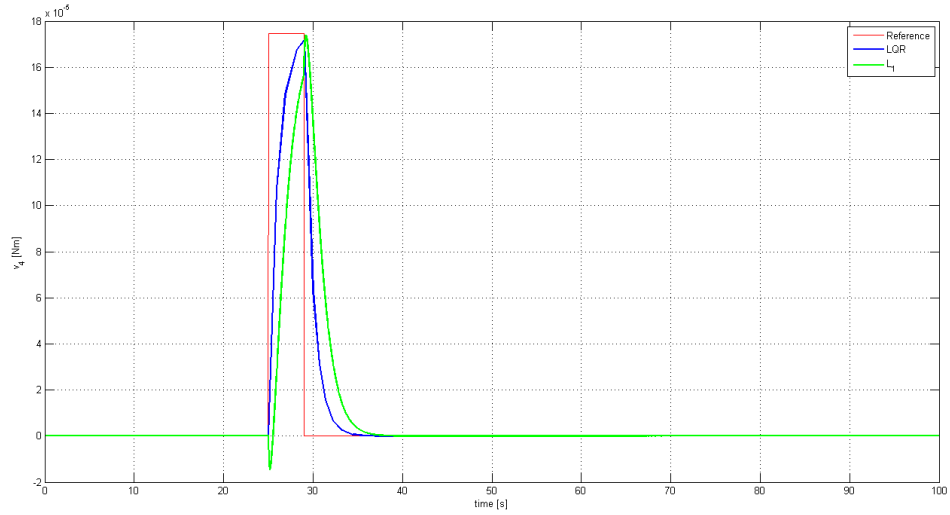

Fig. 33. Closed loop time histories of the virtual input v_4 for both controllers

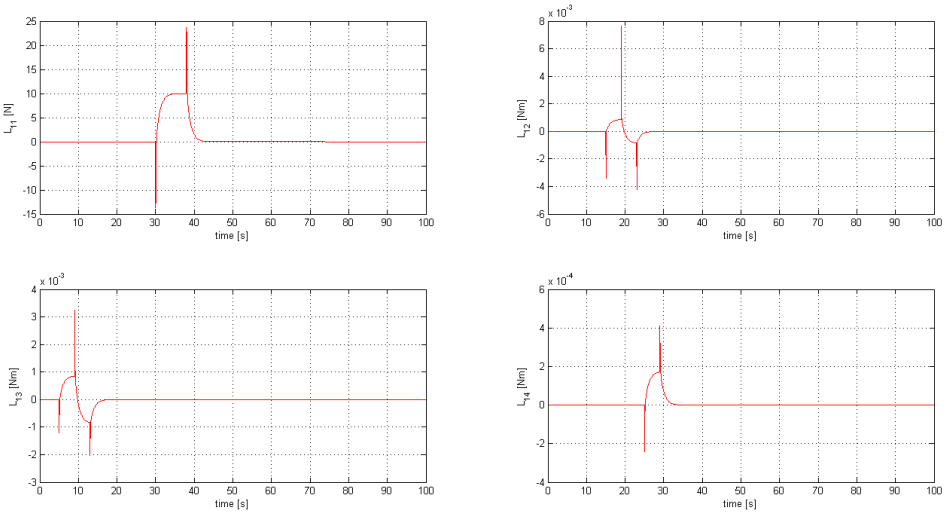

Fig. 34. Time histories of the $\mathcal{L}_1$ controlled inputs for the ideal case

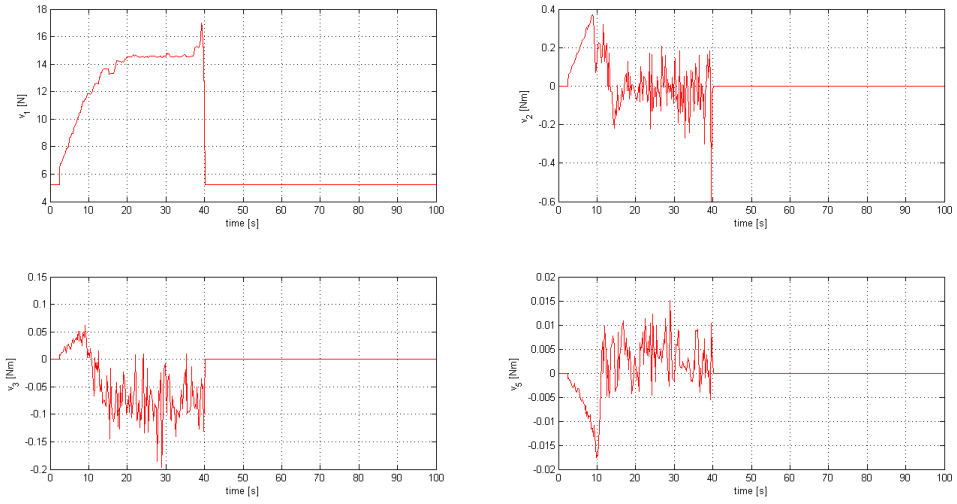

Fig. 35. Time histories of the virtual inputs

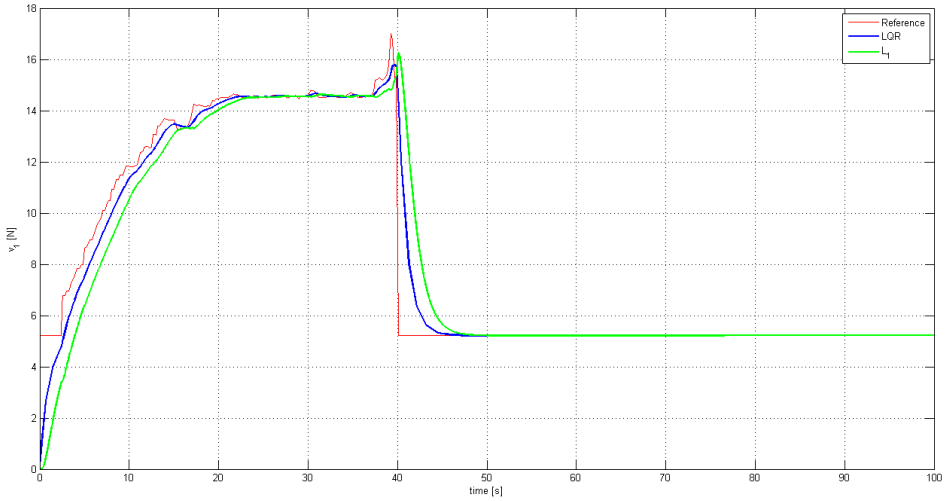

Fig. 36. Closed loop time histories of the virtual input v_1 for both controllers - Experimental inputs

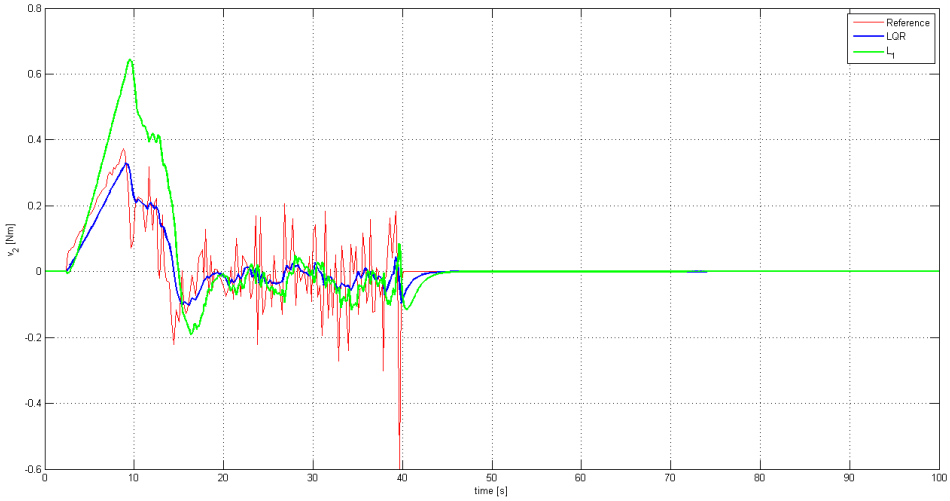

Fig. 37. Closed loop time histories of the virtual input v_2 for both controllers - Experimental inputs

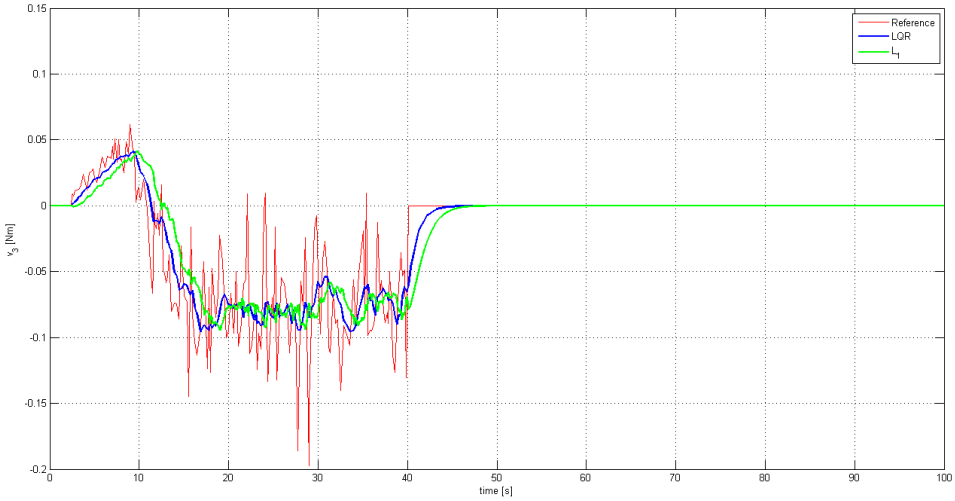

Fig. 38. Closed loop time histories of the virtual input v_3 for both controllers - Experimental inputs

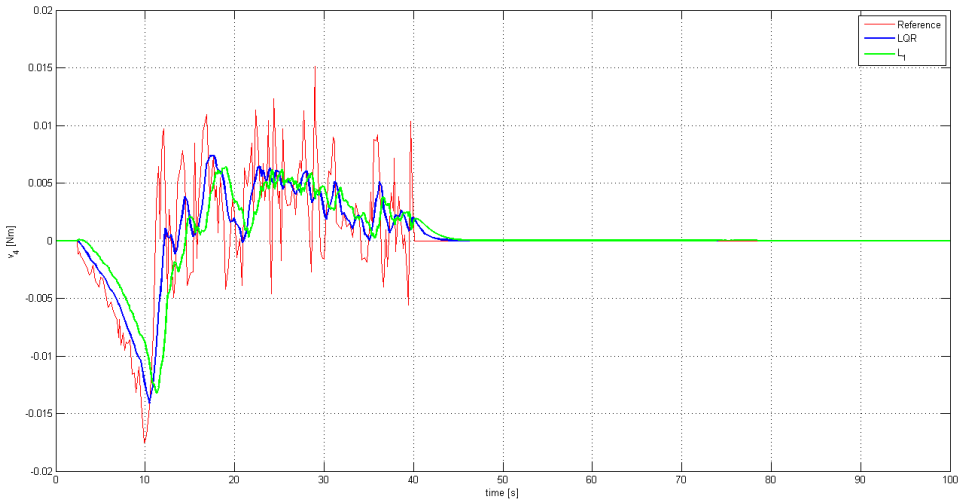

Fig. 39. Closed loop time histories of the virtual input v_4 for both controllers - Experimental inputs

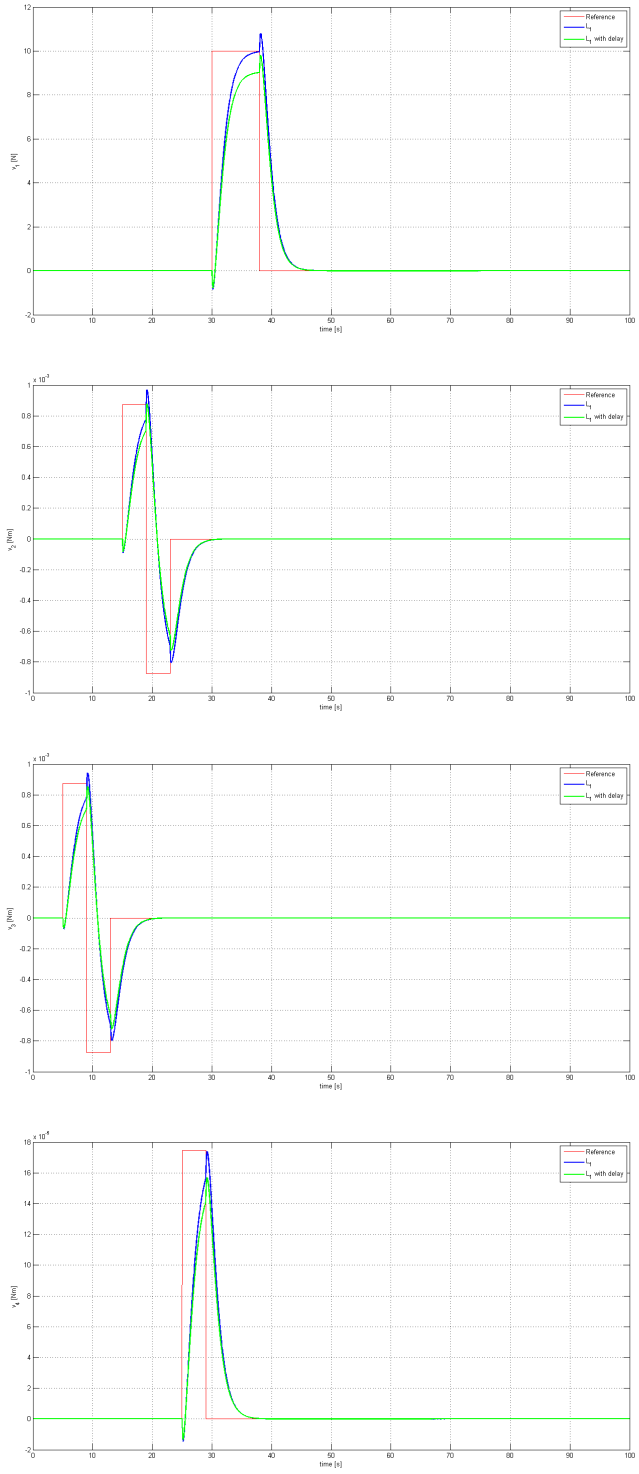

Fig. 40. Closed loop time histories of the virtual inputs v_i with time delay

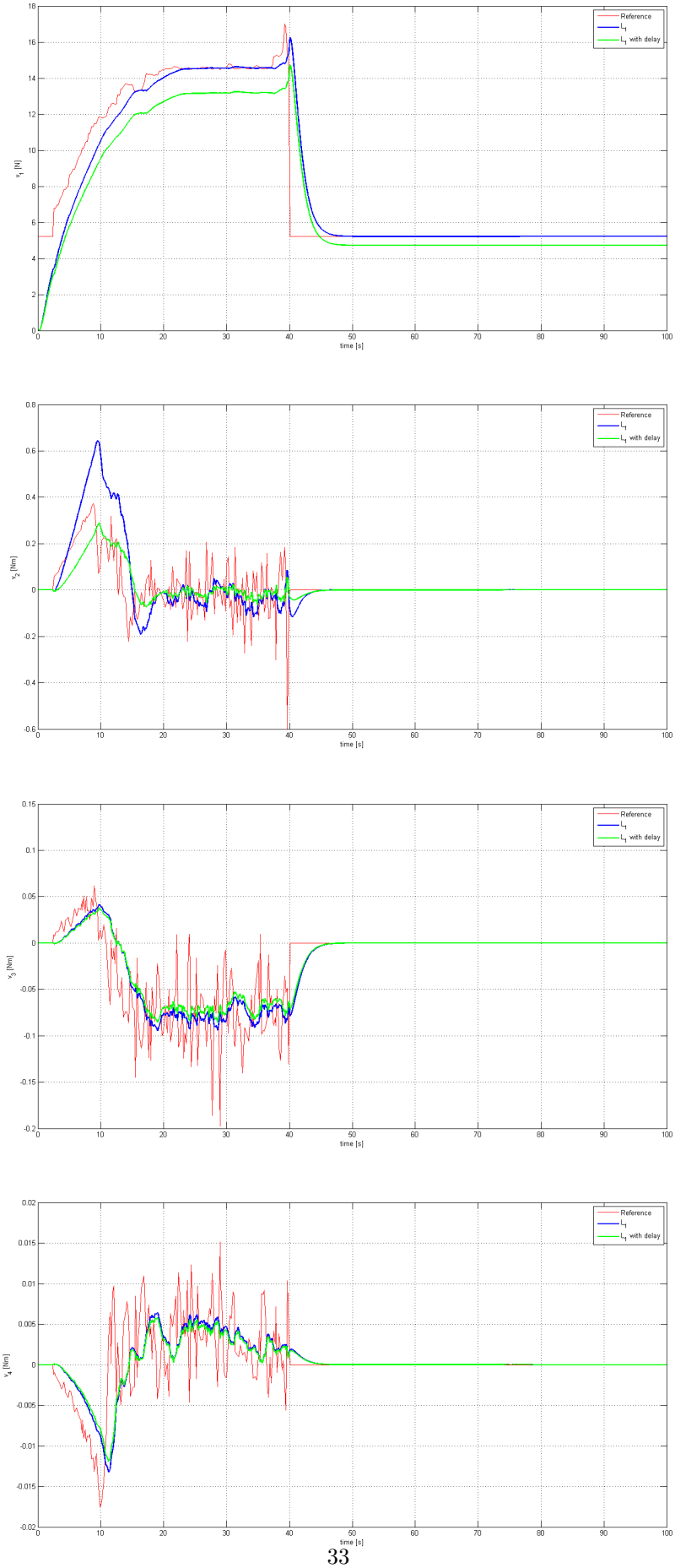

Fig. 41. Closed loop time histories of the virtual inputs v_i with time delay - Experimental inputs

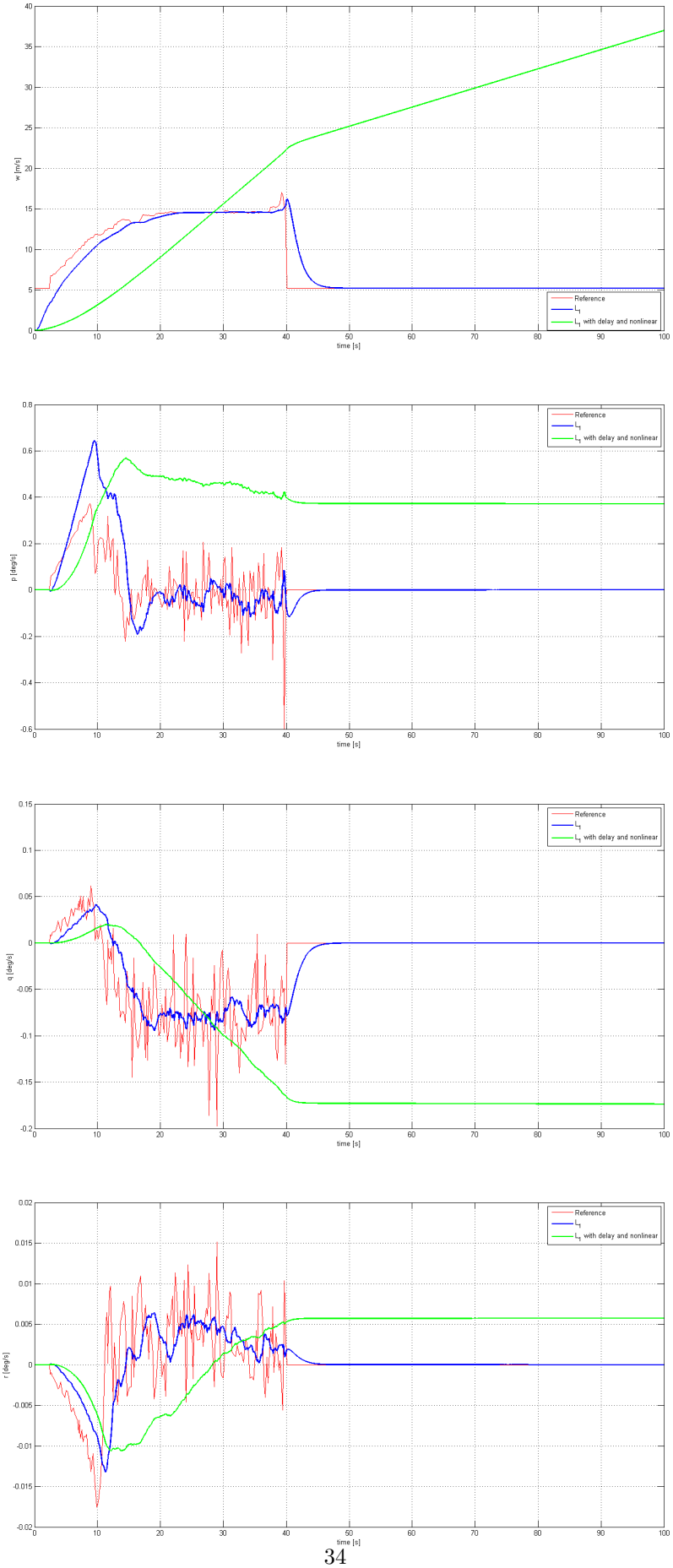

Fig. 42. Closed loop time histories of the nonlinear model with time delay

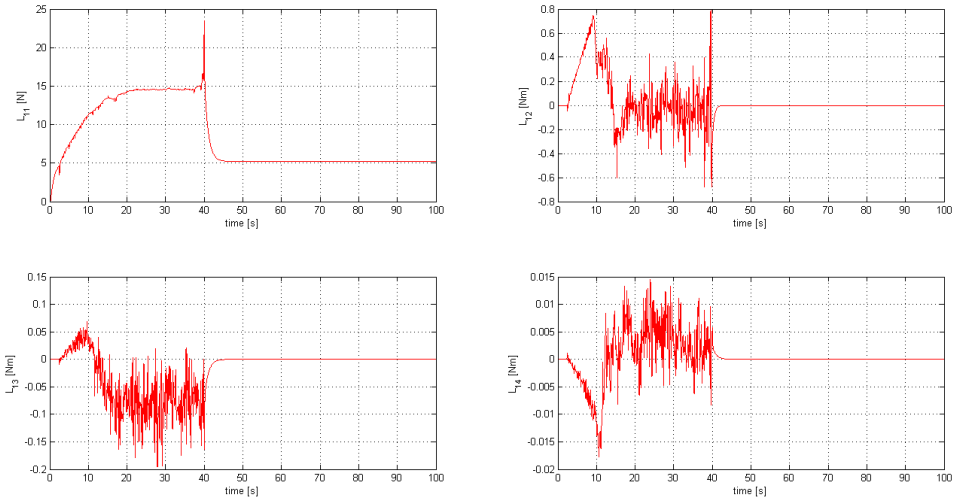

Fig. 43. Time histories of the $\mathcal{L}_1$ controlled inputs for the experimental case

8. CORRELATIONS OF SIMULATIONS AND REAL FLIGHT CONDITIONS

The VICON system is connected to the PC with a protocol called TCP/IP and with the same protocol it communicates with a Matlab-Simulink model. The PixHawk autopilot and the remote controller (for manual piloting) is connected to the computer with a UDP protocol. UDP is used as a way for applications to communicate using a small set of protocol mechanisms. It does not guarantee delivery or packet order as the Transmission Control Protocol (TCP) does. UDP requires the Internet Protocol (IP) to be used as the underlying protocol.

Figure 44 shows the basic setup for a closed loop control experiment in the Spacecraft Robotics Laboratory. The Vicon system tracks the position of the markers on the hexacopter body and the Vicon tracker software computes its the position and orientation. A Matlab script reads, from a TCT/IP port, the position and orientation of the object and send these values through UDP port to the Simulink environment of a different Matlab section in the same computer. The RF transmitter DX7 has the property to operate in the slave mode, which means that two transmiters can be connected through an audio cord and commands from the slave, under PPM protocol, can be transmitted through the master device. In the Simulink environment, the input to the hexacopter is converted to a PPM signal and sent to the audio device. So, this experimental setup is closed by substituting a slave transmitter by the output from the computer audio card. When autonomous flight is performed, the RF transmitter is substituted by the PixHawk autopilot.

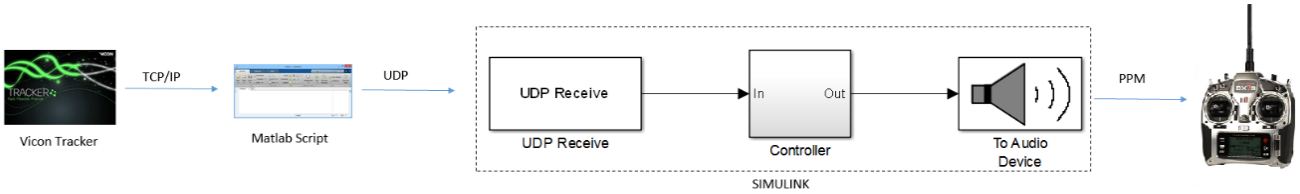

Fig. 44. Closed loop connections

In experimental flights we verified that from the VICON system acquisition and the data sent from Matlab-Simulink enviroment to PixHawk autopilot a delay of about 0.01 s occur. For this reason, in the Section 7 a time delay is considered on the control channel. In that way we have considered a "realistic" case.

9. CONCLUSIONS

The objective of this research (EOARD Grant $14-5007$) is a feasibility study of an $\mathcal{L}_1$ adaptive controller for rendezvous and docking maneuvers, including theoretical background and a comprehensive analysis of simulation results. A model-based design of the system is considered to reduce development time and cost by eliminating the need for early product prototypes. The model-based design of a multi-rotor UAV started from the identification of the model parameters and included and exploration of position estimation techniques using a VICON system. The multi-rotor UAV is used as prototype for technology demonstration.

The nonlinear and linear models of an hexarotor Unmanned Aerial Vehicle (UAV) are identified using a VICON system. The VICON system is considered for measuring the moments of inertia and for evaluating the static gains of the engine (both thrust and torque gains). This approach is chosen for reducing the time of collecting data and to avoid the risk of accidents during flight tests, considering that a stable and robust controller is not yet implemented on-board and it is the scope of this research. Some simulations are performed to validate the implementation of the nonlinear model in the Matlab-Simulink environment.

Two controllers have been implemented: (i) a classical linear quadratic regulator (LQR) and (ii) an $\mathcal{L}_1$ adaptive controller. Both controller performance are validated by simulations. Different cases are analyzed, including simulations of experimental flights. The $\mathcal{L}_1$ adaptive controller is validated not only for the linear model but also for the nonlinear model and for "realistic" cases in which a time dealy and an actuator model are included. Both controllers guarantee good performance. A retuning of the $\mathcal{L}_1$ controller is not required even in presence of time delay and for the nonlinear model. The main contribution of this research is to demonstrate that the proposed control design can stabilize the nonlinear system, even if the controller parameters are selected starting from a simplified linear model. The main advantages of this technique are: (i) the controller can be implemented for both linear and nonlinear systems without parameter adjustment or tuning procedure, (ii) the controller is robust to unmodelled dynamics and parametric model uncertainties. Moreover, the $\mathcal{L}_1$ adaptive controller is able to reduce the measurement noise, due to the low pass filter in the control law. This filter can be useful for improving the data acquisition of the accelerometers and for flight tests combined with a Kalman filter (to have less noisy results).

This feasibility study demonstrates also that the $\mathcal{L}_1$ adaptive controller has good performance for fast dynamics channel but it needs to be connected to a second control channel for the slow dynamics of the system, i.e. speed and altitude variations. As in [8] navigation outer loop parameters are regulated via PID algorithms. One limitation of this controller

is that the linear model has to be known. For this reason we needed to identify the linear model of the hexacopter. This is a limitation because it is a time comsuming process and it is a simplified model of the highly nonlinear real system. For future development a sliding mode controller based on the nonlinear model will be considered. The sliding mode controller must guarantee that the system trajectories reach and maintain a motion on the desired sliding manifold. Moreover, sliding mode control can provide global stability and ensure insensitivity and robustness to system uncertainties and external disturbances. In particular, the sliding mode ability to reject disturbances and parameter variations is useful for space applications. Thus, this controller could be implemented for the Chaser position tracking during the approaching maneuver to a passive vehicle (Target).

10. NOTE: DIFFERENCES BETWEEN THE DEVELOPED AND THE ORIGINAL PROJECT

The original project should considered the following points:

(1) Implementation of the model of a multi-rotor UAV
(2) Development of an $\mathcal{L}_1$-based GNC
(3) Development of a robust control with time varying parameters
(4) Comprehensive analysis of simulation results

The first two points and the last point are deeply discussed in the report and both a linear and nonlinear system is considered. An $\mathcal{L}_1$ adaptive controller is implemented in Matlab-Simulink. A real platform is considered in the overall project and the connection with a PixHawk autopilot (that is the autopilot installed on board) is performed, in order to perform real time simulations (connection with UDP, discussed in Section 8).

For the other points, we can imagine to have matching time varying parameters and a target fixed on ground. A classical linear quadratic regulator (LQR) is implemented and compared with the adaptive controller. A collaborative and fixed on ground target is considered. This is not a limitation on the proposed research due to that, for the most of the literature studies, the target spacecraft does not maneuver by firing thrusters during the rendez-vous and is moving in a predefined elliptical orbit.

Due to time constraints, only some points are deeply discussed and implemented. The original idea was to use only a linear system for the simulation results. In literature is possible to find simple linear model that only marginally describes the real system. For the implementation of an $\mathcal{L}_1$ adaptive controller and to avoid singularity in the controller, a detailed model is usually considered. For this reason, a detailed identification of the multirotor system is considered and proposed in this project to improve the dynamic characteristics.

A comprehensive analysis of different cases is deeply presented in the Section 7. The nonlinear model with time delay and actuator model (that is a model similar to the real platform) is also considered and the $\mathcal{L}_1$ controller performance are validated also for this case.

The only point that it is not considered is the implementation of a guidance algorithm for the docking of a fixed point. The idea is to implement a guidance algorithm that is based on some simplifying hypothesis, according to the flash memory limitation of the autopilot microcontroller. A given set of waypoints will be considered, with assigned North, East and altitude coordinates. Some implementation aspects common to other algorithms available from literature are also considered:

- the trajectory smoother, that makes cinematically feasible the assigned trajectory in terms of speed and turn rate constraints,
- the cross-track error control, to monitor the UAV position with respect to the reference path.
- Look-ahead or proximity distance, to define the minimum distance of the UAV from the next waypoint to begin turning. When the distance between the aircraft and the next waypoint is less than this distance, the waypoint is reached and the aircraft can move to the next waypoint.

We had no time to implement the guidance algorithm and validate it by simulation results.

ACKNOWLEDGEMENTS

Prof. Giorgio Guglieri and Dr. Elisa Capello would like to thank Prof. Marcello Romano and Dr. Hyeongjun Park for providing insightful discussions on the topic of control of UAVs and of rendez-vous and docking maneuvers. Moreover, they would thank Prof. Romano for providing the facilities of NPS laboratory. They would like to thank Dr. Park and Mr. Alessio Grompone for helping performing the experiments in the NPS laboratory.

REFERENCES

[1] K-J. Barsk, "Model predictive control of a tricopter," *Master's Thesis*, University of Linköping, 2012.

[2] F. Beltramini, M. Bergamasco and M. Lovera, "Experiment design for MIMO model identification, with application to rotorcraft dynamics," *18th IFAC World Congress*, vol. 18, pp. 14392-14397, 2011.

[3] K. Bergman and J. Ekström, "Modeling, Estimation and Attitude Control of an Octorotor Using PID and $\mathcal{L}_1$ Adaptive Control Techniques, " *Master's Thesis*, University of Linköping, 2014.

[4] S. Bouabdallah, "Design and Control of Quadrotors with Application to Autonomous Flying, " *PhD disseration*, Ecole polytechnique federale de Lausanne, 2007.

[5] C. Cao and N. Hovakimyan, "$\mathcal{L}_1$ adaptive controller for systems with unknown time-varying parameters and disturbances in the presence of non-zero trajectory initialization error," *International Journal of Control*, vol. 81, pp.1147 -1161, 2008.

[6] C. Cao and N. Hovakimyan, "$\mathcal{L}_1$ Adaptive Output-feedback Controller for non-strictly-positive-real Reference Systems: Missile Longitudinal Autopilot Design," *AIAA Journal of Guidance, Control and Dynamics*, vol. 32, pp. 717-726, 2009.

[7] E. Capello, F. Quagliotti and R. Tempo, "Randomized Approaches for Control of QuadRotor UAVs," *Journal of Intelligent and Robotic Systems*, vol. 73, pp. 157-173, 2014.

[8] E. Capello, G. Guglieri, F. Quagliotti and D. Sartori, "Design and Validation of an Adaptive $\mathcal{L}_1$ Controller for Mini-UAV Autopilot, *Journal of Intelligent and Robotic Systems*, vol. 69, pp. 109-118, 2013.

[9] M. Ciarcià, A. Grompone and M. Romano, "A near-optimal guidance for cooperative docking maneuvers," *Acta Astronautica*, vol. 102, pp. 367-377, 2014.

[10] A. Doblander, D. Gösseringer, B. Rinner and H. Schwabach, "An Evaluation of Model-Based Software Synthesis from Simulink Models for Embedded Video Applications," *International Journal of Software Engineering and Knowledge Engineering*, vol. 15, pp. 343-348, 2005.

[11] A. Douik, H. Liouane and H. Messaoud, "Optimised eigenstructure assignment by Ant system and LQR approaches," *International Journal of Computer Science and Applications*, vol.5, pp. 45-56, 2008.

[12] M.N. Elkhony, "Dynamic Modeling and Control of a Quadrotor Using Linear and Nonlinear Approaches," *Master's Thesis*, The American University in Cairo, 2014.

[13] M. Elsamanty, A. Khalifa, M. Fanni, A. Ramadan and A. Abo-Ismail,"Methodology for Identifying Quadrotor Parameters, Attitude Estimation and Control," *International Conference on Advanced Intelligent Mechatronics (AIM)*, Wollongong, Australia, 2013.

[14] B. Etkin and L. Reid, *Dynamics of Flight: Stability and Control*, New York: John Wiley and Sons (3^{rd} edition), 1996.

[15] O. Flachsbart, and G. Krober, *Experimental investigation of aircraft propellers exposed to oblique air currents*, NASA Technical Report, 1929.

[16] D. Fleischer,M. Beine and U. Eisemann, "Applying Model-Based Design and Automatic Production Code Generation to Safety-Critical System Development," *SAE International Journal of Passenger Cars - Electronic and Electrical Systems*, vol.2, pp.240-248, 2009.

[17] G. Franklin, J. Powell and A. Emami-Naeini, *Feedback control of Dynamic Systems*, Upper Saddler River: Prentice Hall, 2002.

[18] I.M. Gregory, E. Xargay, C. Cao and N. Hovakimyan, "Flight Test of $\mathcal{L}_1$ Adaptive Control on the NASA AirSTAR Flight Test Vehicle," *AIAA Guidance, Navigation and Control Conference*, Toronto, August 2010.

[19] J.S. Hall and M. Romano, "Laboratory Experimentation of Guidance and Control of Spacecraft During On-orbit Proximity Maneuvers," *Mechatronic Systems Simulation Modeling and Control*, A. Milella, D. Di Paola, and G. Cicirelli, Rijeka, Croatia:InTech, 2010, Ch. 11, pp. 187-225, 2010.

[20] N. Hovakimyan and C. Cao, $\mathcal{L}_1$ *Adaptive Control Theory*, Philadelphia: Society for Industrial and Applied Mathematics, 2010.

[21] W. Johnson, *Helicopter Theory*, Princepton: Princepton University Press, 1980.

[22] T. Leman, E. Xargay, G. Dullerud and N. Hovakimyan, "$\mathcal{L}_1$ Adaptive Control Augmentation System for the X-48B Aircraft," *AIAA Guidance, Navigation and Control Conference*, Chicago, August 2009.

[23] T. Magnusson, "Attitude Control of a Hexarotor," *Master's Thesis*, University of Linköping, 2014.

[24] E.H. Moore,"On the reciprocal of the general algebraic matrix," *Bulletin of the American Mathematical Society*, vol. 26, pp.394395, 1920.

[25] K. Narendra and A. Annaswany, *Stable Adaptive Control*, Upper Saddler River: Prentice-Hall, 1989.

[26] R. Penrose, "A generalized inverse for matrices, " *Proceedings of the Cambridge Philosophical Society*, vol. 51, pp. 406413, 1955.

[27] M. Z. Rafat, M. S. Wheatland and T. R. Bedding, "Dynamics of a double pendulum with distributed mass, " *American Journal of Physics*, vol. 77, pp. 216-223, 2009.

[28] A. Roberts and A. Tayebi, "Adaptive Position Tracking of VTOL UAVs," *IEEE Transactions on Robotics*, vol. 27, pp. 129-142, 2011.

[29] G. Szafranski , R. Czyba and M. Blachuta, "Modeling and identification of electric propulsion system for multirotor unmanned aerial vehicle design," *2014 International Conference onUnmanned Aircraft Systems (ICUAS)*, May 27-30, Orlando, FL, 2014.

[30] C. C. Tsui, *Robust control system design, advanced state space techniques*, New York: Dekker Inc., 1996.

[31] J. Villagra and D. Herrero-Perez, "A Comparison of Control Techniques for Robust Docking Maneuvers of an AGV," *IEEE Transactions on control systems technology*, vol. 20, pp. 1116 - 1123, 2012.

[32] A.P. Wang and S.F. Lin, "The Parametric Solutions of Eigenstructure Assignment for Controllable and Uncontrollable Singular Systems," *Journal of Mathematical Analysis and Applications*, vol. 248, pp. 549-571, 2000.

[33] B. West, *Model-Based Design. ECN: Electronic Component News*, vol. 53, pp. 26-27, 2009.

[34] E. Xargay, N. Hovakimyan and C. Cao, "$\mathcal{L}_1$ Adaptive Controller for Multi-Input Multi-Output Systems in the presence of nonlinear unmatched uncertainties," *Proceedings of American Control Conference*, pp. 875-879, 2010.

[35] A. Zulu and S. John, "A Review of Control Algorithms for Autonomous Quadrotors," *Journal of Applied Sciences*, vol. 4, pp.547-556, 2014.

APPENDIX

LIST OF FIGURES

LIST OF TABLES